# Investigation of wave diffusers to scatter the unstirred radiation of an antenna in a reverberation chamber

By

Evangelia Aikaterini Karadimou

Master by Research

University of York, UK
Department of Electronics

January 2013

# Abstract

In a reverberation chamber the direct (unstirred) path between two antennas is the aggregation of the line-of-site path and a number of unstirred specular wall reflections. Ideally these latter reflections should be eliminated in order to control the direct path for multi-path radio simulation applications (Pirkl et al., 2011).

This work describes an experimental programme undertaken to investigate the hypothesis that the contribution of the specular wall reflections to the unstirred energy in a reverberation chamber can be reduced by wave diffusers placed around the specular reflection points on the chamber walls. The wave diffusers will scatter the reflected energy over a wide angular spectrum and increase the energy that is stirred by the chamber's stirrer. Periodic wave diffusers were used optimized for a frequency of 3GHz.

The method is based on a past research method for increasing the mode density in a reverberant screened room. That study found that the electromagnetic field was scattered in many directions by the use of binary pseudo-random phase reflection gratings on the wall of the screened room, while in the absence of the gratings the field was concentrated in particular directions (Clegg et al., 1996). The suggested approach in the present research is to create a grating formed by a binary sequence diffuser which causes diffuse reflection.

Experiments were initially conducted in an anechoic and then in a reverberation chamber. The technique was tested while varying the antennas' heights, polarization and elevation angles, and additionally the orientation of the grating. Furthermore, the power of the line-of-sight component was measured in the anechoic chamber by placing absorbers on the grating and was then subtracted from the total received signal, to

leave the scattered components remaining. The power of the signal reflected from the grating could thus be calculated and compared at the receiving antenna with the power in specular reflection which is observed by using a plane reflector.

In the reverberation chamber the research was based on the effect of the diffusers on the unstirred energy. For this reason the transmitting signal between two biconical antennas was measured, with and without the diffusers placed around the specular reflection points of the room. Parameters like the heights, the polarization and the distance of the antennas as well as the orientation of the diffusers were tested. Measurements in time domain showed significant reduction in the unstirred energy of the cavity.

# Contents

# List of Figures

# Acknowledgements

Firstly, I would like to thank my supervisor Prof. Andy C. Marvin for giving me the opportunity to pursue my studies at the University of York and to work on this project. Thanks to his guidance and his advice I achieve to complete my research. Special thanks are addressed to my thesis advisor Dr. John Dawson who has always been willing to help me with any difficulties in my research.

Moreover I wish to thank all the members of the EMC group in the department of Electronics. All you have contributed to make a very pleasant environment. Thank you for helping me to make myself comfortable since the first day I arrived and for all your help and advice during my master.

My sincerest thanks go out to all my friends that I met in York and made it feel like home. Thank you for all the conversations, the dinners and the parties that we shared. You made this year unforgettable.

I am also deeply thankful to my bosom friend Eleni for her friendship, support and significant help throughout this year. Keep tolerating me!

Finally I would like to thank my family for believing in me, encouraging and support me in many ways in all my life.

# 1

# Introduction

The reverberation chamber offers a cost effective and practical environment to test the performance of electrical and electronic equipment. As far as the communications systems are concerned, this chamber can be used for measuring the basic parameters of antennas such as the radiation efficiency, the total radiated power, the diversity gain, the receiver sensitivity and throughput (Holloway et al., 2006). The use of this shielded room is unique because of the metallic walls and the one or more rotating metallic paddles called stirrers. The highly conductive walls create an environment full of electromagnetic modes and reflections for the electromagnetic radiation (Rosengren and Kildal, 2001). Thus, in the cavity of the reverberation chamber, a multipath environment is created providing a good simulation of the circumstances that antennas are exposed to in the real world (Fielitz et al., 2010). The rotating stirrer changes the boundaries of the electromagnetic field. In this way, the electromagnetic modes change over time and create a uniform statistical distribution.

The uncertainty of the measurements in the reverberation chamber is strongly connected to a basic factor that characterizes the room; the K-factor. The average K-factor quantifies the degree of the line-of-sight (LOS) component present in the multipath environment.

The main source of errors in a reverberation chamber is the unstirred radiation. This radiation follows a path without intersecting the stirrers, creating in this way standing waves. In this case, the power flux density varies widely with location and as a result the statistical uniformity of the energy distribution is destroyed.

The goal of this research is the redirection of the antennas' radiation in a reverberation chamber. For this purpose the use of diffusers was proposed. Our experiments took place in the reverberation chamber located at the University of York in the UK. We investigated a new method of redirecting the radiation of an antenna and reducing the unstirred energy in a reverberation chamber. The idea of this method came from the combination of two previous researches one of which studied the use of phase reflection gratings to increase the mode density in a screened room (Clegg et al., 1996) and the other one focused on the study of the unstirred energy (Pirkl et al., 2011).

This report is divided into six chapters. Chapter 2 provides the basic theoretical background of the multipath environment and the principles of the reverberation chamber. Additionally, a brief description of the previous studies which our method was based on, is given. Chapter 3 describes the use of the diffusers within the reverberation chamber and the theoretical expected results coming from Matlab simulations. Chapters 4 and 5 give the measurements setup and the results respectively. Finally, in chapter 6 we discuss our results and possible future work.

# 2

# Literature Review

One of the most important factors in the life of the modern human is communication. The proof comes from the fact that everyone these days requires new high technology devices that provide wireless access in communication channels from across the world. It has been less than 120 years since Guglielmo Marconi managed to send the first ever wireless communication signal over open sea, this field has developed an astounding rate and today, there are techniques and devices of great technology. For instance, the Global Positioning Systems (GPS) that are based on satellite network provide information of location or time and work under any weather conditions. Cell phones, which are portable devices, communicate via an interface usually using a stationary unit such as the base station. In light of these ever increasing demands, the main research focus of wireless communication systems is based on the optimisation of their quality, coverage and robustness.

The dominant components of these communication systems are the antennas that

may work either as transmitters or receivers. An other fundamental factor that affects the quality of these systems is the propagation path. An antenna is actually a transducer. As a transmitter, it converts the energy of an electrical circuit to electromagnetic waves that are transmitted to free space and vice versa when it works as a receiver. Thus, the role of an antenna is to radiate energy in the form of electromagnetic waves. The electromagnetic radiation is based on the coexistence of both electric and magnetic field components. The electric field is produced by the presence of changing current while the magnetic field is produced by changing electric field according to Maxwell's equations:

$$\begin{aligned} \nabla \cdot \mathbf{E} &= \frac{\rho}{\varepsilon_0} \\ \nabla \cdot \mathbf{B} &= 0 \\ \nabla \times \mathbf{E} &= -\frac{\partial \mathbf{B}}{\partial t} \\ \nabla \times \ \mathbf{B} &= \mu_0 \mathbf{J} + \mu_0 \varepsilon_0 \frac{\partial \mathbf{B}}{\partial t} \end{aligned} \tag{2.1}$$

These two fields are perpendicular with each other and the direction of the propagation, which is defined by the orientation of the transmitting antenna. When these waves are in phase they are called Transverse Electromagnetic waves (TEM).

Ideally, the electromagnetic waves travel from the transmitting antenna directly to the receiving in a straight line. However, there are signals emitted in different angles from the transmitting line even in the case of a directive antenna. These antennas, radiate the greater amount of power in a narrow beam, which means that they work effectively in particular directions.

The propagation of electromagnetic waves can occur through any medium or in vacuum. In the real environment, there are usually many obstacles in the radiation path e.g. tall buildings, lamp posts or other objects which result in multipath propagation. As a result, the finally received signal will be distorted and will consist of many contributing waves from the different propagation paths. Thus, apart from the direct or Line-Of-Sight signal, a lot of other signals - coming from different paths - reach the

receiver. These signals are the results of phenomena that cause phase shifting, constructive or destructive interference and hence fading. The signals' strength decreases as the distance between transmitter and receiver increases. When the magnitudes of the received waves follow a Rayleigh distribution this is known as Rayleigh fading (Stuber, 1996). On the other hand, when there is a strong direct Line-Of-Sight (LOS) component, Rician fading is considered to be the appropriate model of the propagation path (Jayaweera and Poor, 2005).

Reflection, diffraction and scattering are some of the basic propagation mechanisms which might have an impact on propagation in electromagnetic communication systems. Details can be found in the literature (Giger, 1991). The basic propagation mechanisms of electromagnetic radiation are briefly explained below:

Specular Reflection: It happens when an incident wave hits an object with a very smooth surface and a much larger boundary size compared to the wavelength of the radiation. In this case, the direction of the electromagnetic wave changes and the angle of the incident wave is equal to the angle of the reflected wave according to the Law of Reflection.

Diffuse Reflection (scattering): It occurs when an incident wave hits an object with rough surface. This kind of reflection, like the specular one, obeys the Law of Reflection. Thus, while the electromagnetic waves fall on a specific area of the microscopically unsmooth surface, they are reflected in a direction that is determined by the orientation of this specific area according to the Law of Reflection. In this way, the result of diffuse reflection is a random distribution of reflected waves while the orientation of the surface is random distributed. Subsequently, the specular reflection is a special case of diffuse reflection.

Refraction: This phenomenon is observed when a wave crosses the boundary from one medium of propagation to another. Different mediums have different densities and the velocity of the electromagnetic waves is proportional to the density of the medium. Practically, in refraction the direction of the radiation changes when it enters a different medium at a specific angle.

Diffraction: It refers to the case when the waves bend around corners. When the electromagnetic wave meets an object in the propagation path it tends to bend

around it. This fact changes the direction of the radiation but makes also feasible the propagation of the information behind any obstacle or through any gap-hole. This phenomenon is related to the size of the obstacle compared to the wavelength of the radiation.

Absorption: In this case the total energy of the radiated field is reduced. This loss occurs because the radiation passes through media that are not transparent for the nature of the waves and hence they absorb part of their energy.

All these transmitting/receiving systems use different frequencies and are affected by different environments. The need to test the devices in a similar environment to the real one becomes increasingly important. A good solution is to perform the test within laboratories that can simulate the real environment using the different devices (including the antenna) in the same mode as the final user would use it. The traditional antenna measurement facilities like the anechoic rooms and especially the reverberation chambers are becoming increasingly popular for electromagnetic testing.

## 2.1 Reverberation Chamber

The Reverberation Chamber (RC) or mode-stirred chamber was introduced by Mendes (1968). Initially, it was proposed for Electromagnetic Compatibility (EMC) purposes investigating issues of electromagnetic emissions of devices that are subjected to tests. However, it is currently used for many other electromagnetic investigations including shielding and measurements on the antenna efficiency. The Reverberation Chamber is a closed and usually rectangular cavity. The material of the walls is high conductive and causes multiple wave reflections creating a multipath environment. In other words, it is a room used to simulate a real environment where the signal that reaches a receiver is the sum of many interfering waves that come from different scatterers. Since it provides a controlled and repeatable multipath environment, it is the perfect place to evaluate any performance which is impractical to be done in the real world. In order to achieve the representation of many different multipath, the room is equipped with a non symmetric arbitrarily shaped metallic paddle that is rotated changing the geometry of the room. This component is called the stirrer and changes the spatial distribution of

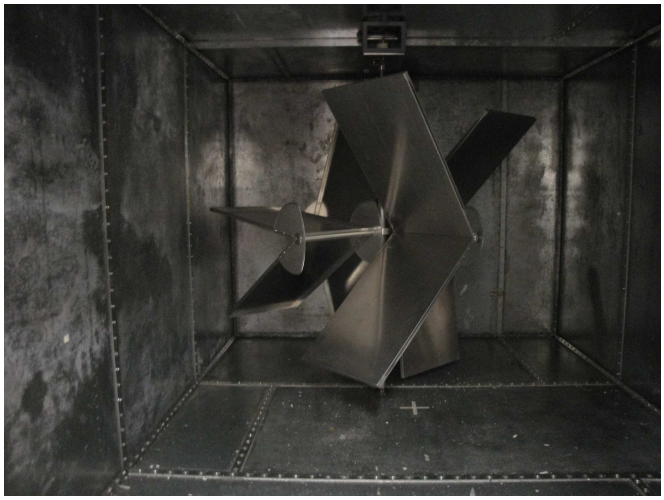

Figure 2.1: Reverberation Chamber at the University of York.

the electromagnetic fields periodically. When averaging over all the possible positions it creates a uniform electromagnetic field (IEC61000-4-21, 2003).

Figure 2.1 shows the reverberation chamber in the department of electronics at the University of York. The dimensions of this chamber are 4.7 m × 3 m × 2.37 m giving a total internal volume of approximately 33.4 $m^3$. The vertical asymmetry stirrer has dimensions of 2 m × 1.2 m (Dawson et al., 2003). The design of the stirrer follows the generally accepted principles of being electrically large at the Lowest Usable Frequency (LUF) and the overall stirrer structure must not be rotationally symmetric (IEC61000-4-21, 2003).

When building a RC it is quite important to take its size into consideration in order to determine its characterization parameters. The size of the cavity and the stirrer should be large enough in terms of wavelength to support several cavity modes at the operation frequency. For instance, the volume of the RC at the University of York is approximately 33.4 $m^3$ which means that it performs well frequencies above 300 MHz (Dawson et al., 2003).The lowest frequency at which a RC complies with the basic operational requirements is called Lowest Usable Frequency (LUF). Despite the importance and the strong connection of this parameter with the size of the cavity, it generally, does not show a clear threshold characteristic (see Serra, 2009, §2.3.7). Therefore, the LUF could be estimated in several ways using empirical definitions (IEC61000-4-21, 2003). One of these defines the LUF in a chamber as the six times cutoff frequency

of a cavity of the same size with the RC under investigation. Although, a lower limit of three times the cuttof frequency could be also accepted if the requirements for the field uniformity are fulfilled. A second way defines the LUF as the frequency that corresponds to the 60th cavity mode so as to yield a statistical homogeneity within ±8dB. Apart from these definitions for the LUF, there are some theoretical models that try to study it analytically. Arnaut (2001) gave a theoretical approximation based on the chamber mode density while Arnaut (2002) found a prediction using a thermodynamic approach and an approximation for the LUF by matching the coherence volume of a quasimonochromatic blackbody radiator with the working volume of a RC.

As mentioned above, the RC is a cavity with high conductive metallic walls which work as wall-mounted antennas, generating an artificial multipath environment. In other words, the RC is a resonant multimode cavity which supports a specific number of modes (cavity resonance), depending on its size, that form 3-dimensional standing wave patterns. If $\alpha$, $b$, $c$, is the length, width and height of the reverberation and $m$, $n$, $l$ are constants representing one mode then, the resonance frequency is defined as (e.g. Shuang-gang et al., 2009):

$$f_r = f_{mnl} = \frac{c}{2}\sqrt{\left(\frac{m}{\alpha}\right)^2 + \left(\frac{n}{b}\right)^2 + \left(\frac{l}{c}\right)^2} \tag{2.2}$$

where, at least two of the constant parameters have to differ from zero.

Theoretically, only when the excitation frequency is equal to the resonance frequency a mode can be excited. However, in reality, there are no lossless cavities and as a result the modes are excited in a certain mode bandwidth $\Delta f$ and all the resonances within the range $f_{mnl} - \Delta f/2 \leq f \leq f_{mnl} + \Delta f/2$ will be excited by the frequency $f$. Each of the resonating modes can be characterized by its $Q$-factor (quality factor), which is the center frequency over the mode bandwidth. This frequency bandwidth is related to the quality factor of the chamber according to the following equation (Price et al., 1993):

$$\Delta f = \frac{f}{Q}. \tag{2.3}$$

This equation states that in a chamber with high $Q$, a small band of frequencies are excited in contrast with low $Q$ cavities where there is greater overlap between different resonant modes.

$Q$-factor is a key quantity to determine the shielding effectiveness and the time constant of the room. It describes the ability of the cavity to store energy and to reverberate. This factor represents how well the chamber reflects the transmitted energy and thus, is affected by any kind of losses in the volume. For instance, the losses from the material of the walls, the apertures and any loading. It is defined as the total energy in the cavity divided by the dissipated energy multiplied with the excitation frequency as follows Hill et al. (1994):

$$Q = \omega U_s / P_d \tag{2.4}$$

where $\omega$ is the excitation (angular) frequency, $U_s$, is the steady-state energy in the cavity, and $P_d$ is the dissipated power.

An other significant advantage that the quality factor provides is that by knowing the $Q$-factor of a RC and therefore the losses in it, it is possible to predict the amount of energy needed to produce a field strength. A high $Q$-factor means that the cavity has low losses and less energy is required for a given field compared with a cavity with lower quality factor and higher losses. Moreover, the $Q$-factor is related with the mode excitation.

The cavity resonances are excited in the room and form the electromagnetic field to which the Equipment Under Test (EUT) is subjected. The electromagnetic waves that transfer energy propagate in transverse modes and the RC as a resonant cavity, accepts only energy at frequencies that correspond to the chamber's resonant frequencies. These waves are described by the Maxwell's equations (see Eq. 2.1).

In the closed cavity of a Reverberation Chamber there are a lot of resonant modes and this causes variations of as much as 40 dB in the wave patterns. Thus, there are regions where the field is small and others where it is large and the spatial distribution of the electromagnetic field is not uniform but highly dependable on the location in the room. However, a statistical uniform and isotropic field is necessary for any kind

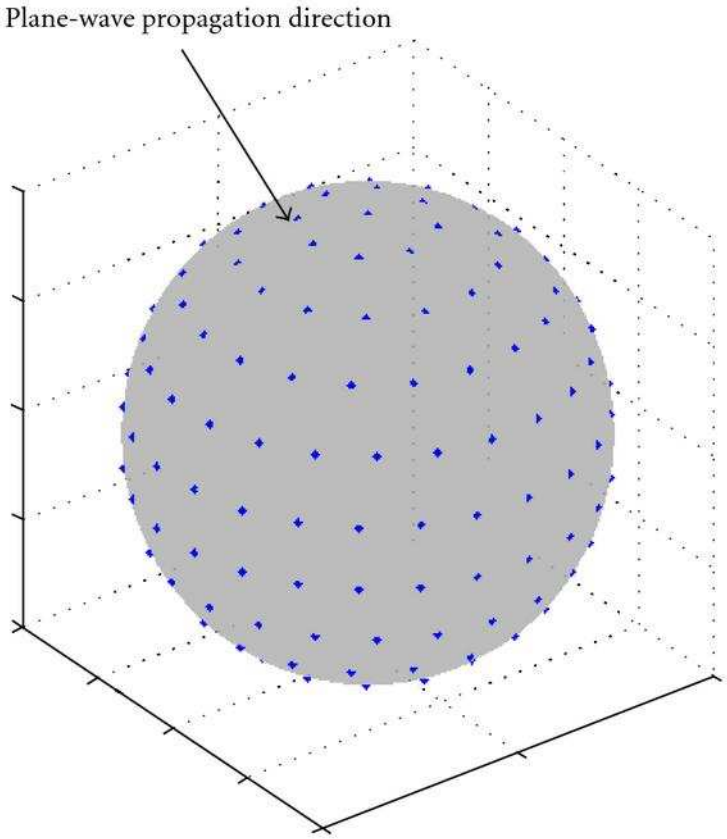


Figure 2.2: Propagation directions of the plane waves over the whole unit sphere. Each point defines a direction of propagation for two plane waves (see Hansen, 2012, Fig.3).

of tests in the RC so that all the sides of an EUT will be subjected to the same field conditions. For this reason, the chamber is equipped with a stirrer that provides mechanical stirring. Continuous or stepwise manner rotation of this paddle causes changes in the geometry of the room. In this way, the boundary conditions alter and different modes are perturbed for every position of the stirrer. This changes the positions of the minima and the maxima in the wave pattern causing a time varying field. Over the course of one revolution of the stirrer all the points are subjected to the same minimum, maximum and average of the field. The field in the chamber becomes uniform while the energy density is the same in all over the volume and isotropic because the energy flow is the same in every direction. In this case, the field can be described by its statistics if the number of modes is large enough. Figure 2.2 shows the propagation directions of the plane waves in the RC. They are uniformly distributed over the whole unit sphere.

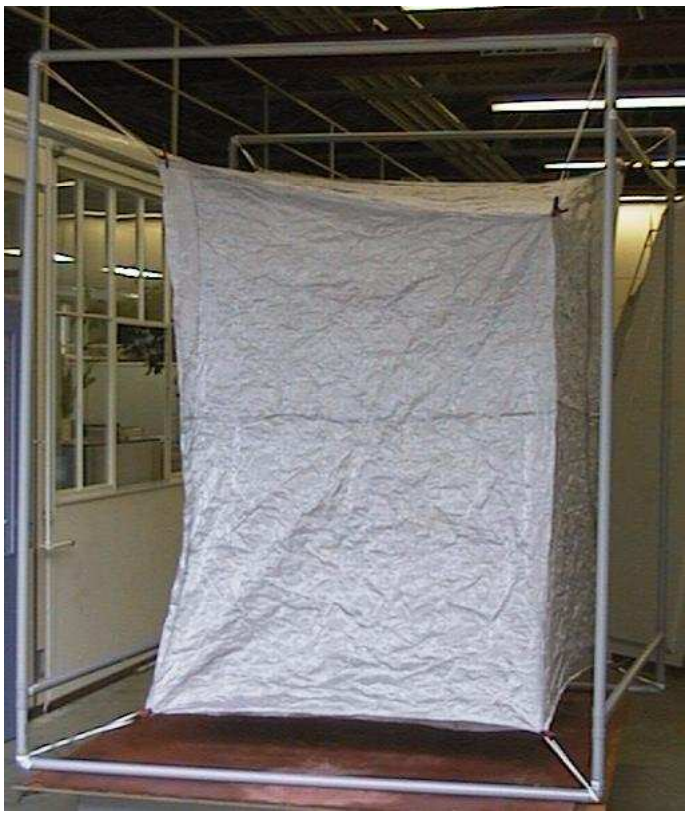

Figure 2.3: The VIRC: a flexible tent irregularly shaped. The field is stirred by moving the walls. The VIRC hanging in strings (Leferink et al., 2000).

Apart from the mechanical stirring there are also other ways to create a statistical uniform electromagnetic field. One of them is using a vibrating intrinsic reverberation chamber (VIRC; Leferink et al., 2000). VIRC is a room with varying angles and vibrating walls made of flexible conducting material. In this case the dimensions of the room change by moving one or more walls or ridges. A photo of a VIRC is shown in Figure 2.3. An other possible way is to use platform stirring Rosengren et al. (2001). In this case the transmitting and receiving antennas are moving in the chamber on a rotating platform. A final alternative way is based on a method that is applied during the data processing. The data of a frequency are processed considering also the data of neighbouring frequency within a specific bandwidth. This method is called frequency stirring (Loughry, 1991).

Figure 2.4: The Anechoic Chamber in the University of York.

## 2.2 The Anechoic Chamber

An other type of chamber that is used for EMC, EMI, antennas tests and many other applications and is used in the present research for reference measurements, is the anechoic chamber. Contrary to the RC, an anechoic chamber is free from reflections. The surfaces in the interior are covered by electromagnetic wave absorbent material and simulate the free space. However, if there are not any absorbers on the floor, the chamber is called semi-anechoic and simulates an open area site. Many types of absorber are available, such as those made using ferrite tiles or pyramidal, carbon loaded foam types. The importance of this room stems from the fact that it provides a special environment free from reflections, isolated from any external noise where there is only the direct path between a transmitter and a receiver. Figure 2.4 shows the anechoic chamber in the University of York. The dimensions of this room are 3.5 m $\times$ 2.3 m $\times$ 2.3 m.

## 2.3 Previous Studies in the Improvement of the Performance of Reverberation Chambers

### 2.3.1 Increasing the mode density

As the use of the Reverberation Chambers has increased over the years high demands are placed on the research about the optimization of their operation. Many solutions have been proposed in order to increase the number of modes in the cavity of the RC, some of them require changes in the geometry of the room while others introduce wall irregularities in the chamber.

Clegg et al. (1996) introduced a new method to increase the mode density in a reverberant screened room in addition to previous methods like mode stirring (e.g. Hill, 1994; Wu and Chang, 1989). This method uses phase reflection gratings based on binary sequences. Placing diffractors on the reflecting walls of a reverberation chamber could be particularly useful in order to increase the efficiency of the room.

The idea came from applications in optics (Schroeder, 1975) and acoustics (D'Antonio and Konnert, 1984). In optics, diffuse reflecting walls are used to scatter the energy and produce a uniform optical energy field while in acoustics, phase reflection gratings are used in rooms as concert halls to improve the sound quality. The use of diffusers has been reported in several studies. Some of them were based on pseudo-random binary maximum-length sequence phase reflection gratings (e.g Schroeder, 1975; Clegg et al., 1996; Petirsh and Schwab, 1998; Petirsch and Schwab, 1999), others on quadratic-residue (e.g. Petirsch and Schwab, 1997; Hoijer et al., 2000) or primitive-root (e.g. Hoijer et al., 2000) designs. Since there were sequences that could increase the mode density for acoustics it was expected that the method would be effective in electromagnetic waves too.

The Clegg et al. (1996) investigation, took place in a physical model of a screened room whose dimensions were 0.9 m $\times$ 0.45 m $\times$ 0.45 m. For the simulation of this room the Transmission Line Matrix (TLM) modelling package was used (Herring et al., 1991). To make things easier, the method was restricted to phase reflection gratings on binary sequences. Figure 2.5 (Clegg et al., 1996) represents an example grating on the wall of the room with the two levels that were used for these sequences and the

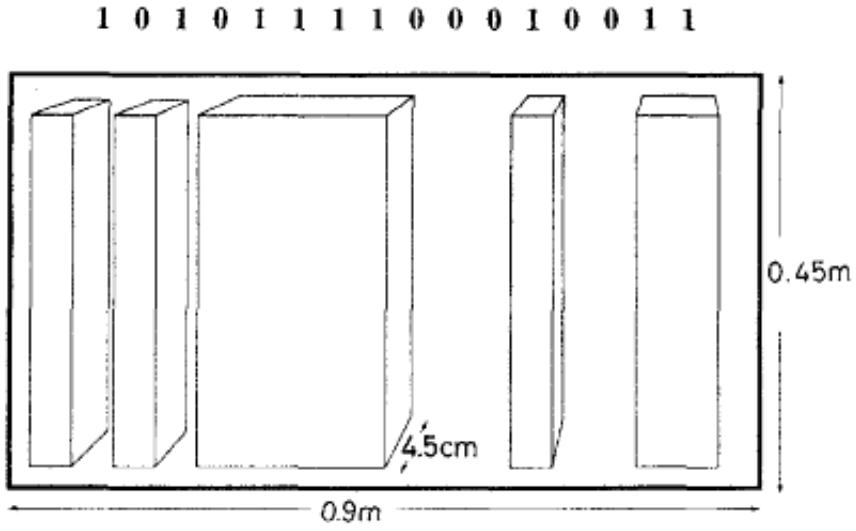


Figure 2.5: Example grating on wall of room (Fig.1, Clegg et al., 1996).

dimensions of the elements.

The number of the modes had been counted in an empty room and it was in agreement for both TLM and physical model. They found that the mode density was increased when the grating was introduced in the room. With this reassurance, the next target was to detect the optimal sequence which would increase the mode density more than any other. For this reason, TLM was used to investigate different sequences. In these simulations, one wall was covered by the sequence and a plane wave was sent towards it. The effect of the different sequences was studied by the far field radiation scattered pattern of reflected wave, given by the following equation (Cartet, 1990):

$$E_f(\theta) = \frac{j\beta_0\alpha(1+cos\theta)}{4\pi R}e^{-j\beta_0 R} \times \int_{-\frac{b}{2}}^{\frac{b}{2}} E_0(x)e^{+j\beta_0 x sin\theta}dx \tag{2.5}$$

R is the far field radius, $b$ is the length of the sequence in the $x$ direction and $\alpha$ is the width of the individual sequence element. The scattered energy, proportional to the direction is given by the equation:

$$P_f(\theta) = |E_f(\theta)|^2 \tag{2.6}$$

where $\theta$ is the angle measured from the specular direction.

In order to detect the optimal sequence, a new measure, $S^2$, was introduced. To define $S^2$, Clegg et al. (1996) considered an ideal isotropic scatterer. The value of $S^2$ for each sequence was defined by the squared deviation of the radiation pattern from the isotropically scattered energy based on the following equation:

$$S_f^2 = \sum_{\theta=-90^o}^{\theta=90^o} \{\frac{P_f(\theta)}{\sum_\theta P_f(\theta)} - \frac{1}{181}\}^2 \tag{2.7}$$

where $\theta$ is the angle in the radiation pattern. The sum in the above equation represents the total power over the particular frequency values for which the equal spread of energy is desirable.

Two were the main results of Clegg et al. (1996), the scattering of the energy in many directions and the increase of the mode density in a screened unstirred room using phase reflection gratings. Comparing the $S^2$ for different sequences they found that the optimal binary sequence is the best as it scatters the energy uniformly in every direction and returns the least $S^2$ value. Their results could be summarized in Figure 2.6 where the effect of the phase reflection grating on the direction of the fields is shown.

### 2.3.2 The problem of the unstirred energy

An other interesting research came from Pirkl et al. (2011). The motivation of this study was the improvement of the accuracy of measurements in a RC. The electromagnetic field in a well-operating chamber is uniform and isotropic; however, in actual chambers the field statistics may differ from the ideal due to the presence of components resulting from multipath propagation that do not intersect the stirrers and thus, they are unperturbed by any mode stirring technique (Primiani et al., 2009). The basic component of a chamber's unstirred wireless channel is usually the direct path between the transmitter and the receiver (e.g. Corona et al., 2000; Holloway et al., 2006) but it is not the only one (e.g. Harima, 2005; Kouveliotis et al., 2003; Primiani and Moglie, 2010).

The research of Pirkl et al. (2011) aimed to interpret geometrically the unstirred multipath in a RC. It was based on the use of wideband aperture measurements where

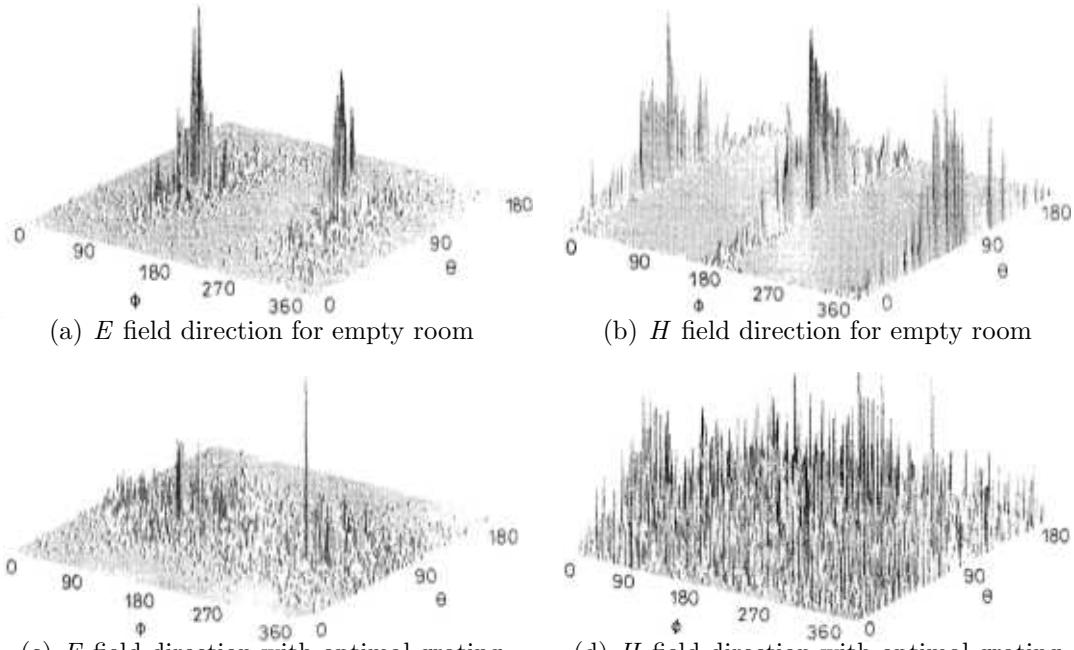


(a) $E$ field direction for empty room (b) $H$ field direction for empty room

(c) $E$ field direction with optimal grating (d) $H$ field direction with optimal grating

Figure 2.6: The summed magnitude of the electric ($E$) and magnetic $H$ field in the empty screened room (top panel). The resulting $E$ and $H$ field directions when the optimal phase reflection grating is included (bottom panel). It is obvious that both fields are scattered into many directions with the effect on the $H$ field being more spectacular (Fig.9-12, Clegg et al., 1996).

a non stationary antenna works as a receiver in order to scan the region around and detect the variations of the signal.

The experiment took place in a RC with two rotating paddles and four pyramidal absorber blocks near the corners of the room to prevent multiple scattering. The transmission characteristics ($S_{21}$) in the chamber were recorder for each position of the scan antenna and each angle of the paddle. Taking into consideration the free-space reflection coefficients of the antennas in order to correct their impedance mismatch of the antennas ($\Gamma_1(f)$ and $\Gamma_2(f)$), the reverberation chamber's wireless channel was defined as (Pirkl et al., 2011):

$$h(f, \mathbf{r}, n) = \frac{S_{21}(f, \mathbf{r}, n)}{\sqrt{1 - |\Gamma_1(f)|^2}\sqrt{1 - |\Gamma_2(f)|^2}} \tag{2.8}$$

The $S_{21}$ data are denoted as $S_{21}(f, \mathbf{r}, n)$ where $f$ represents the frequency, $\mathbf{r}$ denoted the scan antenna's position, and n=1,...,30 denoted the thirty unique paddle angles.

The reverberation chamber's unstirred wireless channel, $\overline{h}(f, \mathbf{r})$, was estimated using the average of the wireless channel for all the positions of the stirrer, $\langle h(f, \mathbf{r}, n)\rangle_n$. Based on this definition, the 2-D space and frequency-dependent unstirred power delay-angle spectrum, was calculated as follows:

$$P_{\overline{h}}(\tau, \mathbf{k}) = |\int\int \overline{h}(f, \mathbf{r}) e^{j2\pi\tau f} e^{j\mathbf{k}\cdot\mathbf{r}} df\, d\mathbf{r}|^2 \tag{2.9}$$

where $k$ denotes wavevector.

The measurements of the unstirred channel for time delay less than 22 ns are illustrated in Figure 2.7 (left). The first pair of pulses indicates the power from the line-of-sight and the ground bounce path. Every pulse symbolizes the power, the delay and the angle of arrival of one or more multipath components. This uncertainty is due to the finite space of the chamber and the fact that the elevation angle was not measured. The measurements of the unstirred wireless channel in the RC were compared with the ones predicted by image/ray theory. Figure 2.7 (right) represents this comparison. Each circle corresponds to the time delay, $\tau_i$, and the angle of arrival of a signal due to the i*th* source image according to image theory (Harrington, 1961). The corresponding multipath component's delay is calculated as:

$$\tau_i = \|\mathrm{R}_i\|/u_p \tag{2.10}$$

where $u_p$ is the free-space propagation velocity of electromagnetic waves and $\mathbf{R}_i$ is a vector pointing from the observation region's center, denoted $\mathbf{r}_{\mathrm{obs}}$, to the $i$th source image's location, $\mathbf{R}_{\mathrm{i}} = \mathbf{r}_{\mathrm{i}} - \mathbf{r}_{\mathrm{obs}}$. Thus, the relevant power contribution to the $i$th source image estimated as:

$$P_i = \frac{\sin^4(\theta_i)}{\|\mathrm{R}_i\|^2} \tag{2.11}$$

where $\theta_i$ is the zenith angle-of-arrival of the $i$th image as determined from $\mathrm{R}_i$. The agreement between the observed and predicted unstirred multipath components of the cavity is also shown. However, there was not absolute agreement in the field of power.

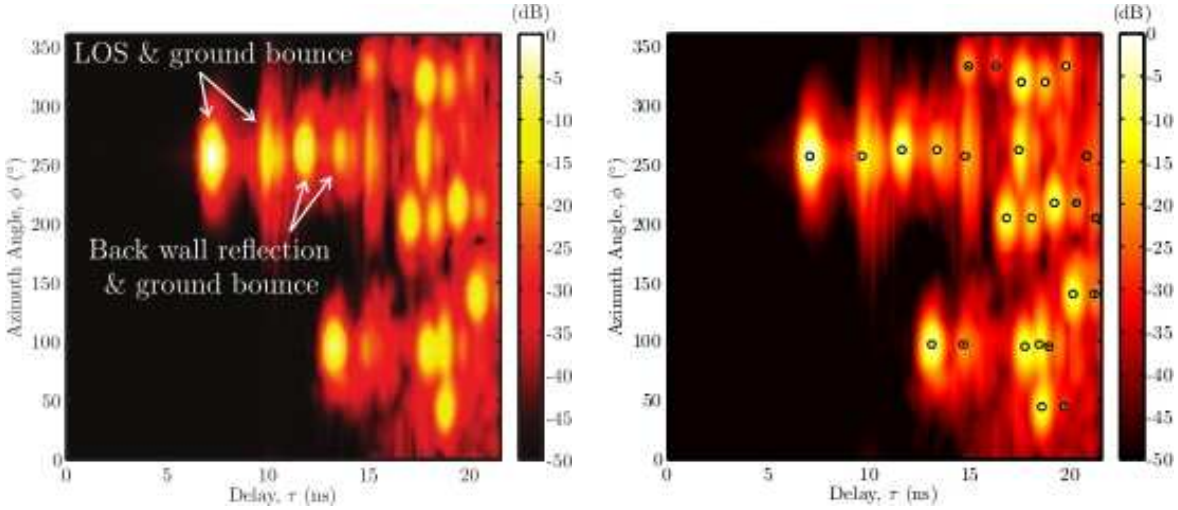


Figure 2.7: Left: The reverberation chamber's early-time unstirred power delay-angle spectrum calculated from measurements of the unstirred wireless channel (Pirkl et al., 2011, Fig.2). Right: Comparison of the unstirred power delay-angle spectrum with the power, time-of-arrival, and azimuth angle-of-arrival of unstirred multipath components as predicted by image theory for a rectangular cavity. The concentric dots identify images whose predicted power differs from the observed power by more than 10 dB (Pirkl et al., 2011, Fig.4).

The eight concentric dots identify the cases where the difference between the measured power and the one estimated by image theory, is more than 10 dB. This fact is due to the overestimation of power in the case of image theory.

In order to optimise the use of this technique, Pirkl et al. (2011) introduced an image-blocking model based on geometry. This model neglects the effect from the real obstacles as well as their images that correspond to multipath components that intersect any object in the RC. The real scatterers in the cavity were modelled with hemispherical caps as shown in Figure 2.8. As far as the stirrers are concerned, the diameter of the used caps was smaller than the cylindrical volume of the paddle. This choice was made because the stirrer's swept volume near the axis is more effective for the obstruction of the ray paths than near the periphery. Figure 2.9 depicts the results after applying the image blocking model. The error rate was reduced from $51 \pm 7\%$ to $22 \pm 4\%$.

The importance of this study is summarized to the geometrical interpretation of the unstirred channel in a RC and the connection of this with the stirred field model. Many techniques have already been introduced like the orientation of directional antennas in a great distance (e.g. Holloway et al., 2006; Choi et al., 2010) in order to reduce the

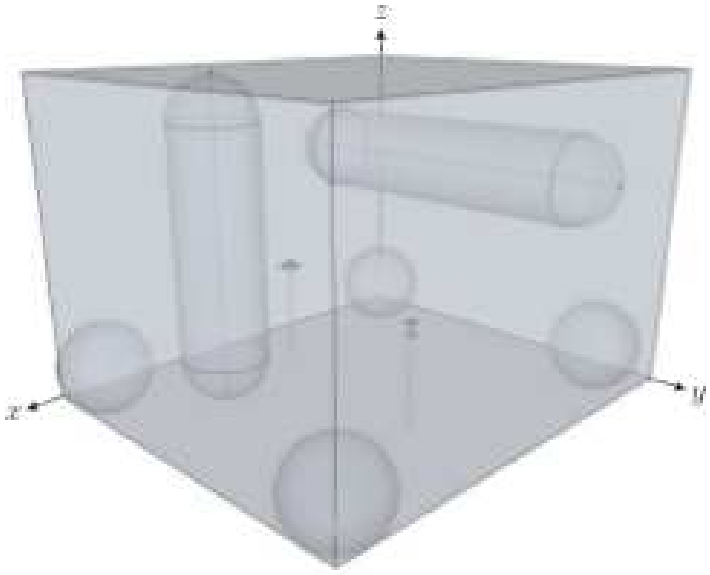

Figure 2.8: Diagram of the simplified problem geometry used with the image-blocking model of the unstirred wireless channel (Fig.6, Pirkl et al., 2011).

unstirred energy. The image-blocking model proved that in this case the LOS path will be attenuated; on the other hand this could increase the unstirred path rays with angles of arrival corresponding to the main beam of the directive antennas' beams. Progress concerning the use of directive antennas, could be achieved if the main beam of these is turned towards the stirrer (Lunden and Backstrom, 2007). Moreover, (Pirkl et al., 2011) indicated the importance of a large cross-sectional area for the reduction of unstirred energy instead of the swept volume of the stirrer. In other words, using multiple large wall-mounted planar stirrers in a RC could be effective in diminishing the unperturbed by stirring propagation paths in the cavity (e.g. Corona et al., 1996; Harima, 2005).

## 2.4 Motivation and Purpose of this Research

The measurements in the reverberation chambers return sequences of power levels which are used to estimate the parameters of the equipment under test. Despite the field inside the chamber is statistic by nature, the accuracy of the estimations depends on how well the excited modes are stirred inside the RC.

Pirkl et al. (2011) showed that the unstirred energy is one of the main factors of the uncertainty associated with the measurements in the cavity of the RC. Different

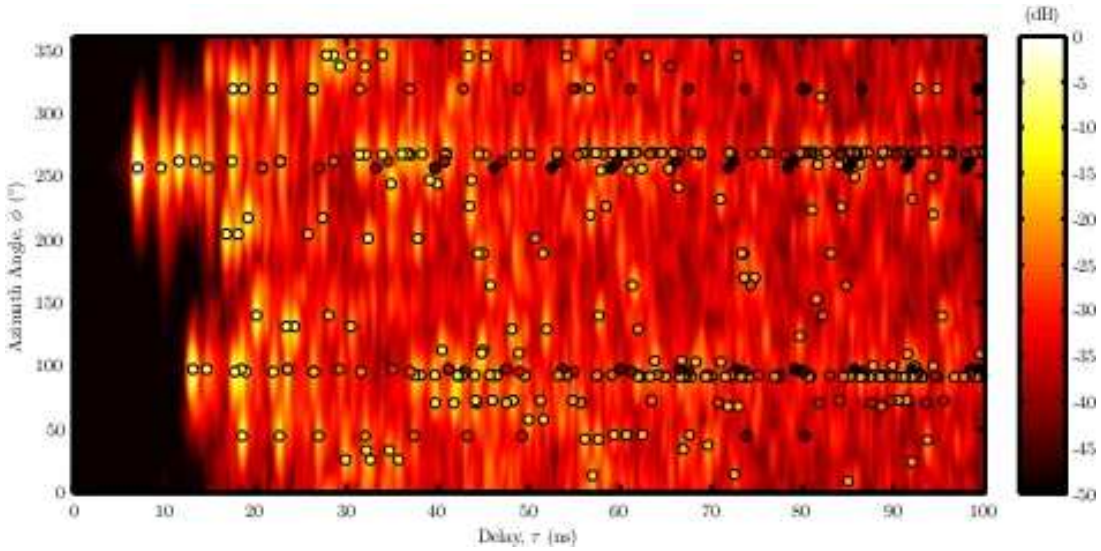


Figure 2.9: The observed unstirred power delay-angle spectrum overlayed by dots indicating the power, time-of-arrival, and azimuth angle-of-arrival of unstirred multipath components as predicted by the image-blocking model (Fig.7, Pirkl et al., 2011).

stirring techniques are proposed by which an improvement of the accuracy is achieved. Some models have proposed the increase of the number of stirrers in the room, while others suggest that stirrers should match the longer of the height or width dimension of the chamber. Other methods, based on the position and the orientaion of the antennas have been also proposed (e.g. Peng et al., 2011; Lunden and Backstrom, 2007). The orientation of the transmitting antennas has significant influence on the radiation in the RC. In order to reduce the unstirred energy, antennas are usually oriented towards the stirred. Also, a good solution is to keep a larger distance, compared to the test frequency wavelength, between the transmitting and the receiving antenna.

However, these methods are strongly connected with the equipment (e.g. stirrers, antennas) that is used in the chamber and they work only under specific circumstances (e.g. orientation, distance). This fact raises the need for a new method that will reduce the unstirred energy in more general cases regardless the exact measurement setup of the experiment.

Clegg et al. (1996) manage to use binary pseudo random gratings in order to increase the mode density in a screened room by scattering the energy. Using this idea, in this thesis a new method for the reduction of the undesirable unstirred energy and generally the scattering of the energy using diffusers is proposed. When the radiation

of an antenna meets the sequence of the scatterers - diffusers it changes its direction. As a consequence, the probability for the scattered radiations to intersect the stirrer, increases. Moreover, even for the radiation that does not impinge the rotating paddle, its amplitude will be smaller than the original one due to the scattering.

# 3

# Diffusers

Tests for electromagnetic immunity and emissions work best when located inside chambers where ambient noise levels are low and test signals are contained. In order to characterize a chamber suitable for such tests, it must fulfill specific requirements concerning the field homogeneity. Anechoic or mode stirred chambers of different sizes can satisfy these requirements (e.g. Crawford et al., 1986; Spiegelaar and Vanderheyden, 1995). An alternative solution is to cover the walls of the chamber with diffusers (e.g. Petirsch and Schwab, 1997; Schroeder, 1985). Simulations have shown that this method improves the homogeneity in rooms. Combining the different methods we can further improve the results. Petirsch and Schwab (1997) achieved to increase the field homogeneity combining the methods of the varying shape room with the acoustic diffusers.

As it was mentioned in Section 2, the fields in a reverberation chamber are statistically distributed. Among other characteristics the quality factor ($Q$-factor) is of

interest. The efficiency of the reverberation chamber is strongly correlated with the $Q$-factor which in turn depends on the amount of the unstirred energy. The lower unstirred energy the better the $Q$-factor is and as a result the efficiency of the chamber is improved. Similarly, the room's efficiency is affected by the number of modes $N$. In order to improve the mode density over different ranges of frequencies, previous studies (e.g. Clegg et al., 1996; Petirsch and Schwab, 1999) combined the mode-stirred chamber with different types of diffusers. Petirsch and Schwab (1999) used acoustic Schroeder diffusers. On the other hand, Clegg et al. (1996) tried different sequences of gratings while the best sequence for electromagnetic waves may differ from the acoustic ones.

Based on these ideas, we performed computer simulations to investigate if the same method also works for redirecting the radiation of the antenna and reducing the unstirred energy in the RC. After these simulations and based on their results, we created the diffusers that are used for the present research.

## 3.1 Diffusion over different frequencies

In acoustics, the acoustical quality of rooms is improved by using scattering elements, called diffusers. The incident sound wave is scattered in all the directions so that a diffuse sound field is generated. Schroeder (1975) proposed a construct of diffusers based on the Maximum Length Sequences (MLS). This idea was based on optics theory where, the far-field scattering can be approximately predicted by taking the Fourier transform of a surface. In this way the power spectrum and surface scattering are closely correlated. The advantage of the MLS is the generation of a flat power spectrum at all frequencies (Cox and D'Antonio, 2009). This principle of diffusing can be also applied in electromagnetics. In this case, the diffusers are made of highly conducting material that corresponds to ideal hard materials in the acoustical case (Petirsch and Schwab, 1999). On the other hand, the idea of diffusion is also used in optical wavelength where the integrating sphere has diffuse reflecting walls to achieve a uniform optical energy density from a scatterer inside the sphere. Light entering the sphere is multiple scattered by the inner surface with high level of total diffusion to all the points. This

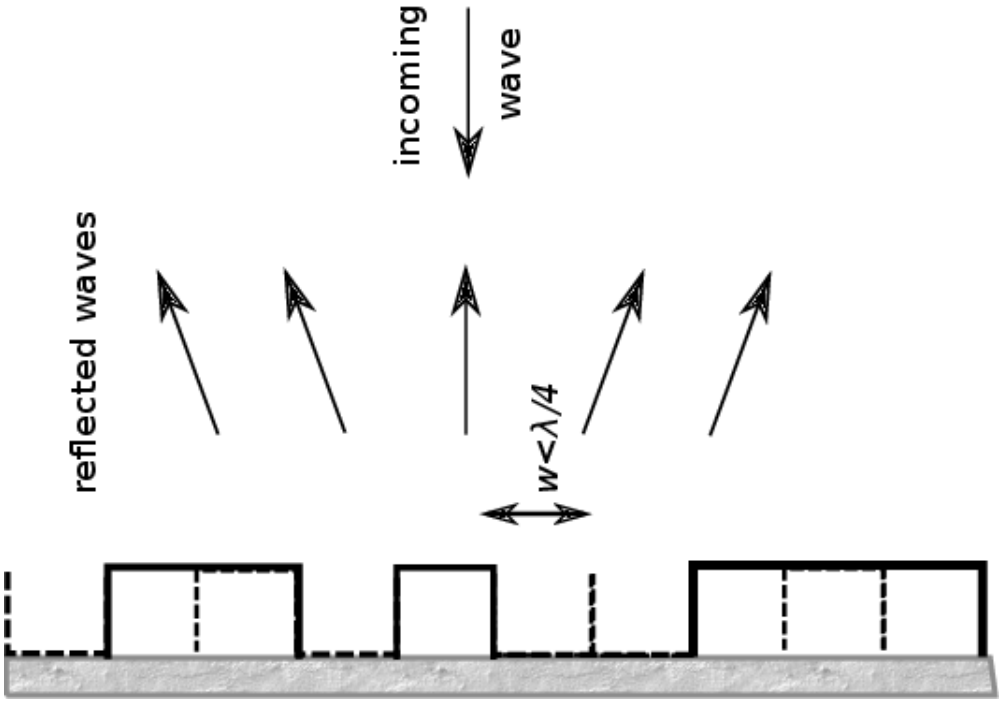


Figure 3.1: Principle of a diffuser.

makes makes an integrating sphere acting like a diffusers, minimizing the effects of the original direction of light.

Figure 3.1 shows the principle schematics of a maximum length diffuser (Schroeder, 1975). The incoming wave reaching the diffusers will be scattered to various directions, depending on their surface geometry. For the demonstration of these diffusers strips of material with two different depths are used, placed according to an MLS. The maximum depth of the diffuser and the width of the elements are smaller than or equal to a quarter of the wavelength ($\lambda/4$) of the design frequency. The efficient frequency range of the diffusers is rather limited, one octave above the design frequency where they exhibit specular reflection. The schematic of a maximum length diffuser is demonstrated in Figure 3.2. In this example, similar to Figure 3.1, a single period of MLS surface is presented based on the sequence *[-1 +1 +1 +1 -1 -1 -1 +1 -1 -1 +1 +1]*. One of their main advantages are the easy construction and their smaller overall volume. The orientation of the diffusers related to the polarization of the incident field determine the efficiency of the diffusers.

Figure 3.2: One period example of a maximum length diffuser according to the sequence *s =[-1 +1 +1 +1 -1 -1 -1 +1 -1 -1 +1 +1]*.

## 3.2 Matlab Simulations

In theory, there are many methods which produce exact solutions of the wave equation provided that a few simple assumptions are valid. These methods allow the direct computation of the scattering parameter from the modeled diffusers. Mathematically exact solutions, however, require high computational cost especially for complicated methods with large structures and despite their reliable and trustworthy result makes the accurate prediction even more difficult. Therefore, there is a need for a more simplistic approach, which aids physical understanding and provides very fast predictions.

In this section we do the assumption that the diffusers work as an arrangement of infinity point-like scatters. As an approximation is analogous to the systems often considered in antenna design, crystallography and general array theory (e.g Balanis, 1982; Hammond, 2001). This consideration describes the scattering behaviour due to the array shape while, at the same time, it does not take into account the influence of shadowing due to neighbouring objects. Ignoring the boundary conditions, we need a

model where each individual scattering point simulates the scattering behaviour.

Here, we use a model of periodic surface diffusers, which consists of a series of wells of the same width, each having a depth of a quarter wavelength and individual reflection coefficient but constant across each element. Each element may then be represented as a point scatterer situated at its centre, with reflection coefficient determined by the element type. The diffuser may be presented as a spatially varying impedance surface. In this case, the reflection coefficient for each point-like element with a corresponding $d_n$ well depth could be given by the impedance of the element

$$R_n = \frac{1 + icot(\beta d_n)}{1 - icot(\beta d_n)} \tag{3.1}$$

where $\beta = 2\pi/\lambda$. In the case of plane surface the reflection coefficient is $R_n = 1$.

The basic setup for a surface diffuser is depicted in Figure 3.3, where a 1D diffuser similar to that of Figure 3.2 is shown as an example. Based on this arrangement, we assume a sequence of $N$ point scattering elements spaced w $= \lambda/4$ apart and an incident electromagnetic wave $E_0$ depending on frequency through $\beta_0 = 2\pi f/c$, arriving from angle $\phi_0$. The source location, $S$, is described by its polar coordinates $r_S$ and $\phi$, the source distance and angle of incidence respectively. The scattered radiation is obtained from the receiver in distance $r_R$ and at an angle of reflection given by $\theta$. By convention $\theta = 0^o$ is considered to be the direction normal to the surface, with the scattered field being limited to $0^o \leq \theta \leq 90^o$.

The received radiation is the result of the interference effects of the scattered components from the diffusers and depends on the receiver's angle and the frequency. The amplitude and the phase of the reflected wave change due to the reflection coefficient $R_n$. The contribution from element number $n$ is expressed by the transfer function $H_n$, which relates only to the reflection coefficient and the delay.

$$H_n = R_n \exp(-i2\pi f \tau_n) \tag{3.2}$$

Assuming a far field model, the distance to the receiver does not have to be known, as the difference between the paths is given by the distance between the elements and

the observation angle. The signal from the source to the receiver may follow different paths; one through $r_1 + r_2$ and another through $r_3 + r_4$, and interference occurs at the receiver due to differences between the phase shifts. When the incident angle changes from $\phi_o$ to $\phi$, the length of the path increases by a factor $\Delta r_\phi$ into $r_3 = r_1 + \Delta r_\phi$. This factor can be estimated from the $Nw$ along the $x$ axis. Respectively, the length of $r_4$ is smaller that the $r_2$ one, $r_4 = r_2 - \Delta r_\theta$, as the scattered angle changes from $\theta o$ to $\theta$. The differences in the path lengths could be summarized as:

$$\begin{aligned} r_1 - r_3 &= \Delta r_\phi, \quad \Delta r_\phi = Nw\sin(\phi) \\ r_2 - r_4 &= \Delta r_\theta, \quad \Delta r_\theta = -Nw\sin(\theta) \end{aligned} \tag{3.3}$$

The delay from the first element to the n$th$ element becomes:

$$\tau_n = \frac{n\Delta r}{c} = \frac{nw\sin(\theta)}{c} \tag{3.4}$$

The transfer function can be now expressed as the combination of the reflection coefficient and the path delay for each element. The total value of the transfer function will be given by summing the contributions of the $N$ number of elements.

$$H = \sum_{n=1}^{N} H_n = \sum_{n=1}^{N} R_n \exp\left(-\frac{i2\pi f n w \sin(\theta)}{c}\right) \exp\left(-\frac{i2\pi f n w \sin(\phi)}{c}\right) \tag{3.5}$$

The model we described above was implemented in MATLAB and tested for several different sequences and angles. The MATLAB implementation is given in Appendix A. For the following results we use a source distance of 1.5m (like the one that we use for our experiments) and radiation of 3GHz frequency where we expect our diffusers to work more efficient based on their chosen dimensions. Firstly, we test if our particular sequence does succeed in reducing the scattering factor comparing to other random sequences. Figure 3.4 shows the normalized scattering factor as a function of angle of the receiver, when the transmitter is at $120^o$ (or $-30^o$ from the normal) position and for $N = 10$ elements within the diffuser. Three different cases are investigated, one without diffusers (blue line), one with diffusers based on the *[+1 -1 +1 -1]* sequence

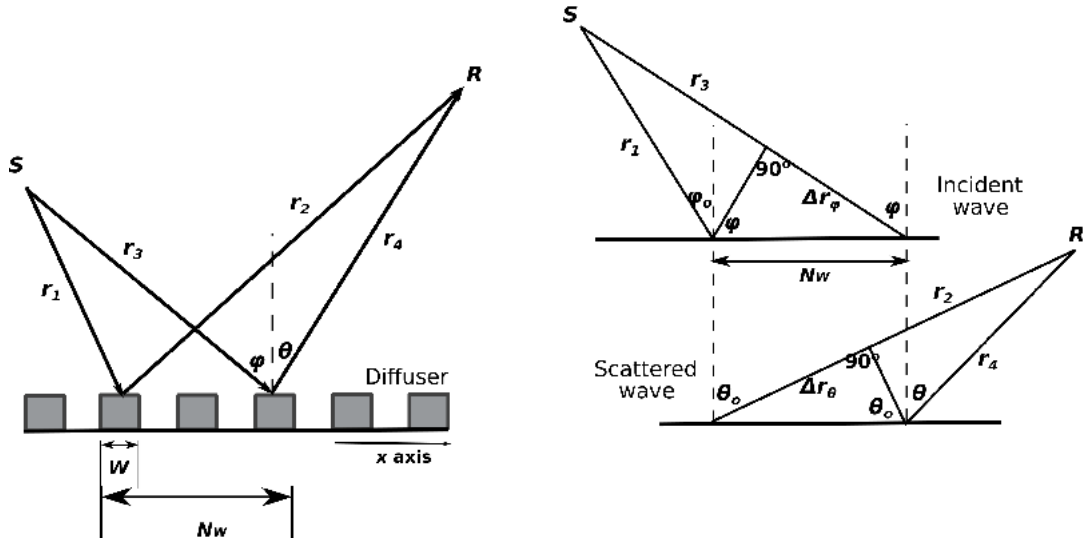


FIGURE 3.3: The scattering from the diffuser cause interference at the receiver. To the right is shown details of incident and scattered waves in order to calculate the difference in path lengths.

(red line) and one with random sequence of diffusers (green line). It is obvious that all cases with diffusers reduce dramatically the specular reflection at $60^o$. Despite the random sequence seems to work well for some specific angles the best overall results are achieved using the proposed *[+1 -1 +1 -1]* sequence. However, even in this case, it seems that for received angles higher than $\sim 110^o$ the scattering factor is comparable to the specular reflection or even higher. For this reason, we test the model for different emitting angles.

Figure 3.5 shows the prediction of our simulations for different emitting angles. Although the specular reflection is reduced for all the cases where diffusers are used, the results are not the same good for all the observed angles. The highest difference is observed around the specular reflected angle. Moving away from this angle both cases (with and without diffusers) return comparable scattering factors and their difference minimizes. Based on these results, we expect, during our experiment, to see the higher differences for frequencies around to 3GHz.

## 3.3 Diffusers development

A diffuser may be defined as any objected in the volume of a space that alters the propagation of an incoming wave that promotes diffuse reflections and/or a diffuse

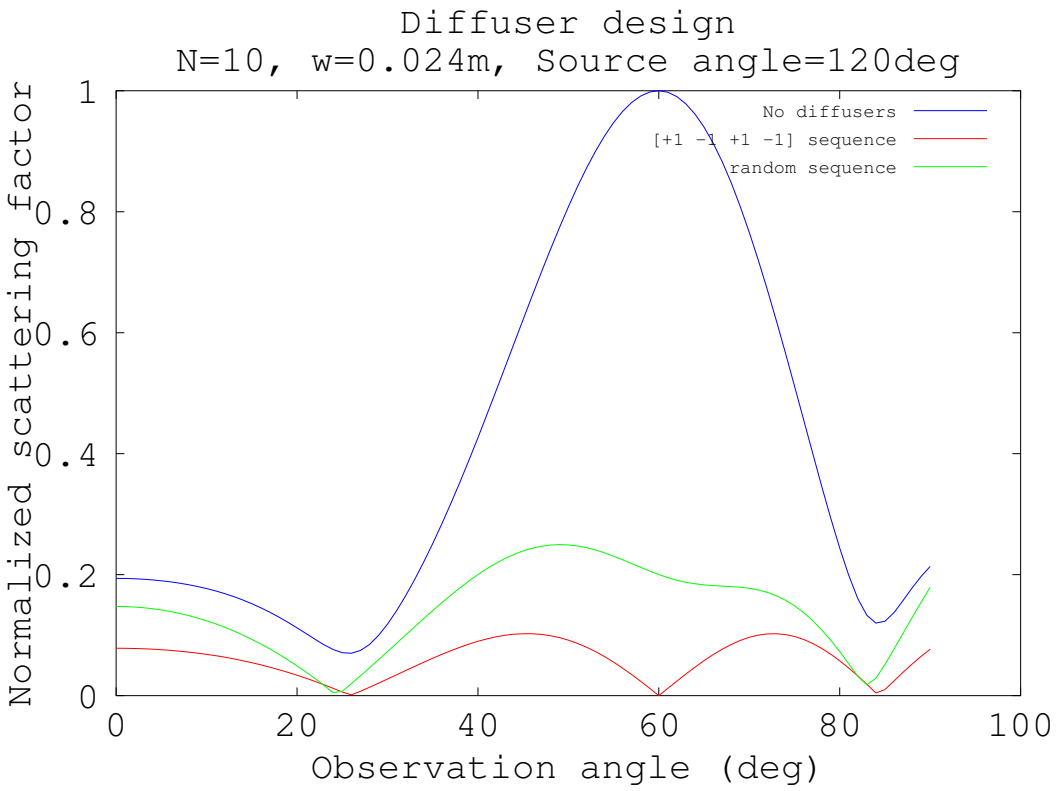


Figure 3.4: Normalized scattering factor for emitting angle $\theta_e = 120^o$. Blue line represents a flat plate with out diffusers, red line diffusers based on *[+1 -1 +1 -1]* sequence and green line diffusers based on random sequences.

field. A simple surface diffuser for example is a structure of two levels which promotes diffuse reflections to scatter the reflected energy, helping reduce unwanted artefacts that result from strong unstirred energy in the case of the reverberation chamber.

In the case of planar diffusers, the surface varies in one direction only as the example in Figure 3.2. Assuming the extruded dimensions are large enough relative to wavelength, scattering in one dimension is only produced. Therefore, the receiver and the source have to simply lie on the plane whose normal is parallel to the extruded dimension.

The design of a diffuser will essentially be limited by size, which in turn is determined by available space. One constraint of these structures is that their placement cannot interfere with a room's functionality. In the context of the work presented here the main limitations raised by the size of the chamber and the distance between the antennas. For this reason, during the development of our diffuser contractor we took into account not only their efficiency for our measurements but also the dimensions of

the chambers we used during our experiments.

As it has been mentioned before, MLS diffusers constitute an easy construction occupying at the same time a small overall volume. One of the simplest MLS diffusers sequence is *s =[+1 -1 +1 -1]*. Taking into account that the main source of the unstirred energy is the strong specular reflection and based on the results of our simulations where maximum reduced specular reflection achieved using the above sequence we developed a uniform sequence of diffusers based on *s =[+1 -1 +1 -1]*.

For our structure orthogonal aluminium tubes of 1m length, 25mm width and 25mm height were constructed. The length of the diffusers was chosen in order to fit well in the chamber. Although the original idea was to place the diffusers vertically to incident polarization of the antennas, the 1m length permits us to rotate the construction in order to test its efficiency also for different incident polarization. Using a width of 25mm we are able to use a large enough number of diffusers (about 20) in the space within the antennas. Based on these dimensions we expect a maximum efficiency at 4×width wavelength. The diffusers were placed periodically on a steel plate in equal distances to their width (25mm) where the position '+1' represents the existence of a tube while the '-1' position represents an empty space on the plate. The elements retained their position on the plain reflector due to the existence of magnets in the interior. Figure 3.6 shows the developed diffusers structure.

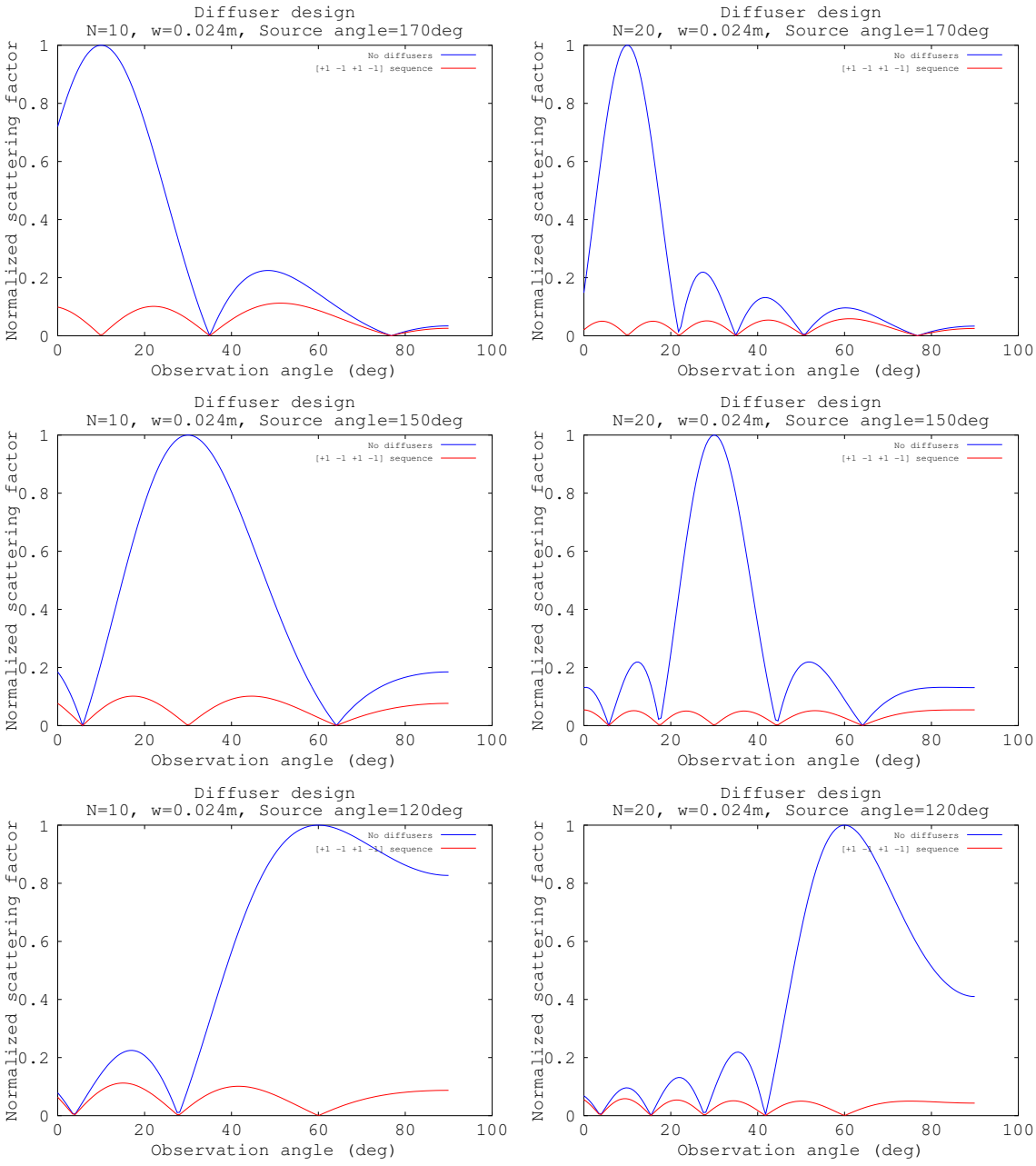


Figure 3.5: Normalized scattering factor for different emitting angles and number of wells within the diffuser. Blue line represents a flat plate without diffusers while the red line represents diffusers based on the *[+1 -1 +1 -1]* sequence.

Figure 3.6: 1m $\times$ 1m optimised orthogonal diffusers constructed according to the sequence $s = [+1\ -1\ +1\ -1]$ .

# 4

# Measurement Setup

## 4.1 Measurements in the Anechoic Chamber

All the considerations done in the previous chapter need to be validated by measurements. In addition, in order to determine the importance of the diffusers in the reduction of the unstirred energy, several measurements are needed to be studied under different circumstances. Before examining the effect of the sequence of diffusers on the unstirred energy in the reverberation chamber, it was important to test it and study the results in a more controlled environment. The anechoic chamber, where there are no reflections, was considered to be the most appropriate place for this.

The setup of this experiment is based on the use of two ridged horn antennas that were available in the laboratory and are shown in Figure 4.1. Both the transmitter and the receiver, were connected to the ports of a Vector Network Analyzer (VNA) that was placed outside of the anechoic chamber.The VNA was the source of the transmitting

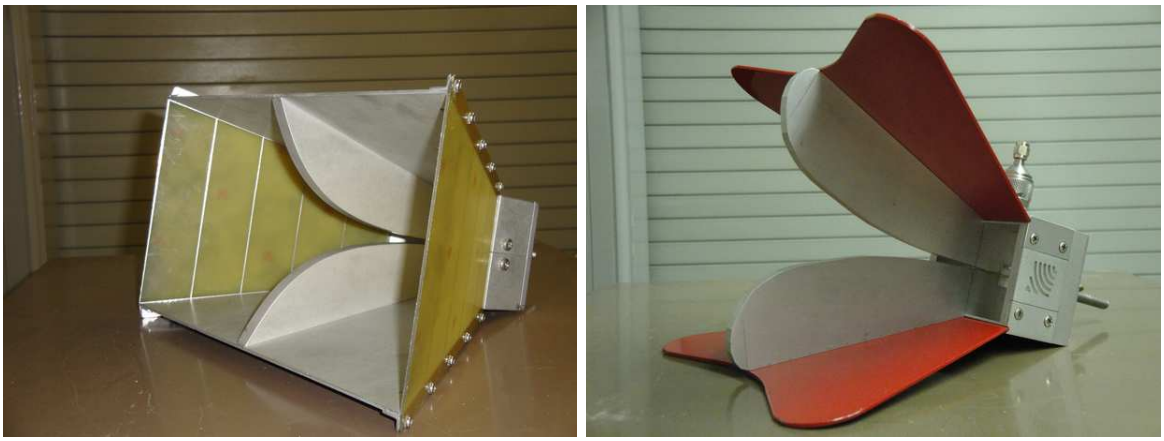

Figure 4.1: The double ridged waveguide horn antennas that were used in the anechoic chamber. The left figure shows the transmitter and the right one the receiver.

signal while, at the same time, it was working as the recorder of the measurements to the connected computer. At the beginning of every experiment, it was important to calibrate the VNA over the frequency range of interest in order to eliminate any possible errors in the VNA (e.g. systematic errors that are caused by imperfections of the instrument) and any cable effects.

As we explained in the previous chapter, there are two parameters which affect the received signal after the scattering, the frequency and the observational angle. Our transmitter, covers a frequency range of 1.5 - 8.5 GHz. On this way, we were able to test the effect of the frequency to our results and if our motivation to demonstrate diffusers of $\lambda/4$ width and depth was correct. In order to have a complete record of results, it was also important to test the method with the antennas at different angles. For this reason, both the transmitter and the receiver were placed on a wooden frame that allowed setting each component at a particular angle independently. The angles were defined by the geometry of the frame.

The goal of the test in the anechoic chamber was to inquire the performance of the diffusers or, in other words, to investigate if by using the diffusers we can scatter the energy to all the directions. This is feasible if we compare the reflected energy from a plane reflector with that one scattered from the diffusers. However, the measured signals included also the component that reached the receiver through the direct path which had to be subtracted (vector subtraction) for our study. For this reason, it was originally necessary to measure the direct path by placing absorbers on the floor

(a) Placing absorbers on the floor to measure the signal from the direct path.

(b) Placing the diffusers on the floor to measure the reflected signal.

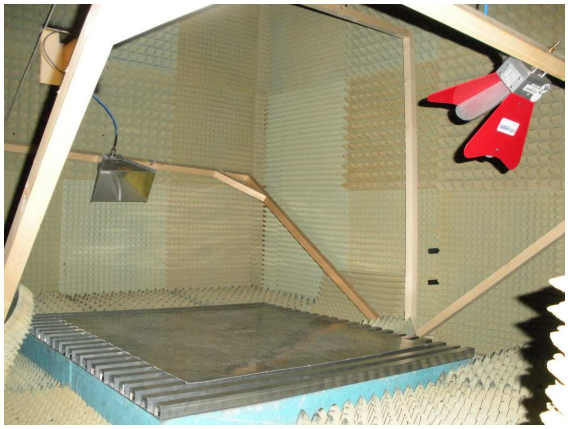

(c) Placing a plane reflector on the diffusers to measure the reflected signal.

Figure 4.2: The three stages of the experiments in the anechoic chamber

between the antennas as is shown in Figure 4.2a.

In Figure 4.2b, the diffusers are placed on the floor between the antennas. Eventually, a plane reflector (steel plate) was placed on the sequence of the diffusers to cover them and cause specular reflection as shown in Figure 4.2c. In all these cases, the S-parameters were recorded, particularly the S21 parameter that indicates the signal that reaches the receiving antenna.

In order to study the efficiency of the sequence broadly, it was important to check the reflected energy for different circumstances in the chamber. We did it changing the basic parameters of the system concerning the height, the angles, the polarization of the antennas and finally the orientation of the diffusers. The results are presenting in chapter 5.

## 4.2 Measurements in the Reverberation Chamber

After testing the sequence of the diffusers in the anechoic chamber the next step was to study its performance in the reverberation chamber. This chapter features several details about this experiment.

The method was tested in the reverberation chamber at the University of York. The dimensions of this room are 4.7 m $\times$ 3 m $\times$ 2.37 m and it contains a vertical stirrer shown in Figure 4.3.

As the main goal of this research was to detect how the diffusers affect the unstirred energy of the room, the measurements had to be taken with the stirrer rotated continuously. This is because the unstirred energy of the wireless channel is estimated by the average of the stirrer positions in the reverberation chamber Pirkl et al. (2011).

The two ridged horn antennas that are characterized by high directivity, were replaced by omni-directional circular biconical antennas in order to detect the reflected signals coming from as many directions as possible in the reverberation chamber. Both the antennas work properly from 1GHz to 10GHz and are presented in Figure 4.4.

The method was again based on the difference between the reflected signal from a specular reflection and the diffusers. The transmitter and the receiver were placed in the room on bases made of polystyrene, which is a wave-transparent material, one

Figure 4.3: The stirrer in the Reverberation Chamber at the University of York.

opposite to the other so that the direct path did not intersect the stirrer. The source of the transmitting signal was, as in the case of the anechoic chamber, a Vector Network Analyzer (VNA). The transmitter was connected to the port 1 of the VNA and the receiver to the port 2 through the ports on the wall of the chamber. In this way, the transmission coefficient S21 between the antennas and therefore the power at the receiver was recorded to the connected computer.

In the beginning of every experiment, after calibrating the VNA and connecting the antennas, the stirrer controlled by a computer, started rotating continuously with a constant speed. This paddle was able to do a complete rotation ($360^o$) in 6400 positions. That means that the difference between two positions corresponds to $0.056^o$. For our experiments the step of the stirrer's rotation was 64 which means $3.6^o$. For every one of the total 100 (6400/64) stirrer positions, 1600 measurement points of the averaged

Figure 4.4: The omni-directional circular biconical antennas that were used in the reverberation chamber. The left figure shows the transmitter and the right one the receiver.

S21 parameter coming from the VNA were recorded for a specified frequency range. These measurements, coming from averaging over all the stirrer positions describe the unstirred channel of the RC.

The diffusers were placed on the metallic surfaces of the cavity at positions that cause the dominant reflection components as explained in chapter 3. For instance, on the floor between and behind the antennas, on the walls behind them and the ceiling. To identify the specific reflections we used the time domain facility available on the VNA. As a result, it was possible to match the peaks of this diagram with the corresponding radiation path according to the time of arrival.

Figure 4.5 depicts one of the experiments performed in the RC with the diffusers placed in 6 panels in 45 degree orientation each and Figure 4.6 shows the corresponding time domain response from the VNA. The first peak indicates the signal that reaches the receiver at 4.6nsec having travelled distance 1.3790m and represents the signal that comes from the direct path. The distance between the antennas is 1m, however this difference is explained if we consider the electrical length of the connections of the antennas. The second one, at 8.6620nsec has coverded distance 2.5968m. This peak is the reflection component from the floor between the antennas (1.2m+1.2m).

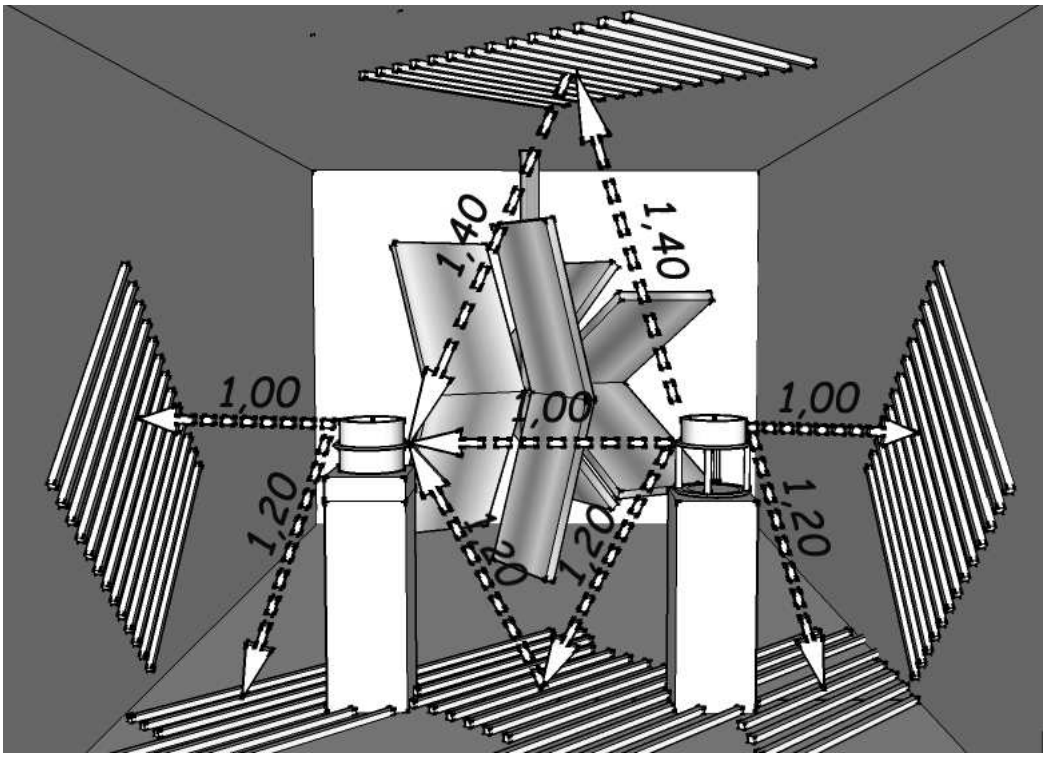


Figure 4.5: Diagram of the Reverberation chamber with the diffusers placed around specular reflection areas.

Placing the diffusers at this area, there is a reduction of 9.761dB. Similarly, equivalent reduction of 6.93dB is noticed at the peak of 11.174ns (3.3499m). This corresponds to the radiation that reaches the receiver after been reflected from the walls behind the antennas. Analytically, as Figure 4.5 shows, the paths that the radiation covers are the 1m one from the transmitter to the back wall and the 2m path from this point to the receiver. At the same time, the radiation covers the 2m path from the transmitter to the wall behind the receiver and the 1m path to the receiver. Finally, the peak at 20.150sec is reduced by 12dB and represents a signal that has travelled 6.0408m following a path that intersects more than one sequence of the diffusers in the chamber. For example, 1.2m distance from the transmitter to the floor behind it, 1.2m from the floor to the wall behind the transmitter, 1m to the trasmitter, 1.2m to the floor between the antennas and finally 1.2m to reach the receiver.

The frequency range is one of the parameters that were examined during the experiment. Originally, the frequency range was from 1.5-8.5 GHz. While testing the method it was considered useful to narrow gradually this range around the crucial frequency, that according to our expectations and due to the dimensions of the diffusers, would

optimize their performance. However, considering that the frequency is reciprocal of time, narrowing the frequency range decreases the resolution in time domain. This makes difficult the distinction of the different reflection components of the propagation path. For this reason it was significant to approach the frequency of the diffusers but to keep also a sufficient level of resolution degree for time domain.

Apart from the frequency range, our method was tested for different heights and polarizations of the antennas and also for different orientations of the diffusers. All these cases are presented in chapter 5.

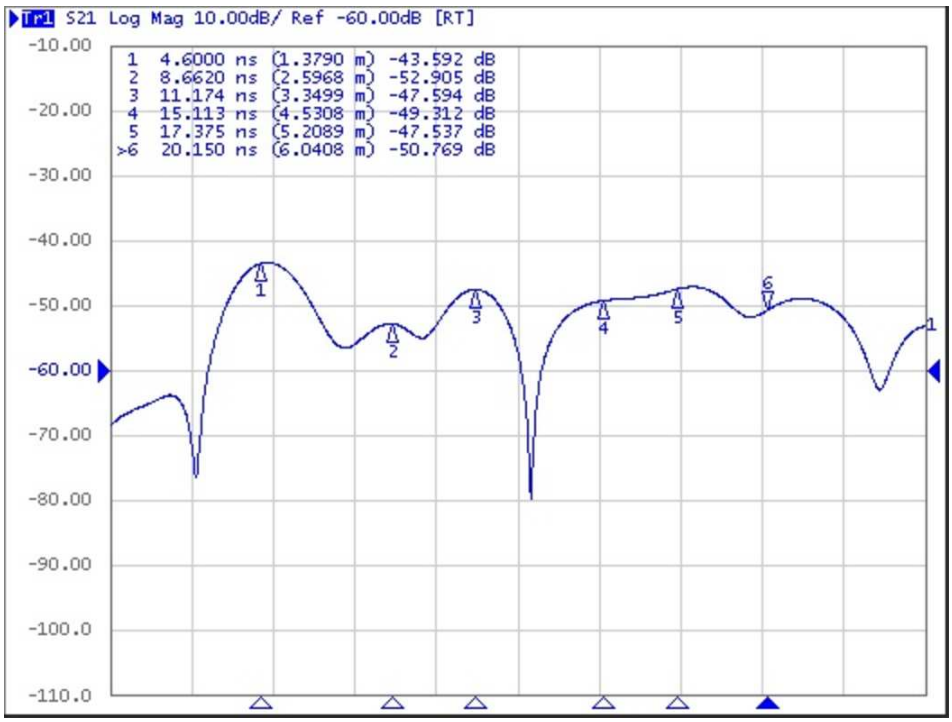


(a) Time domain response in the empty reverberation chamber.

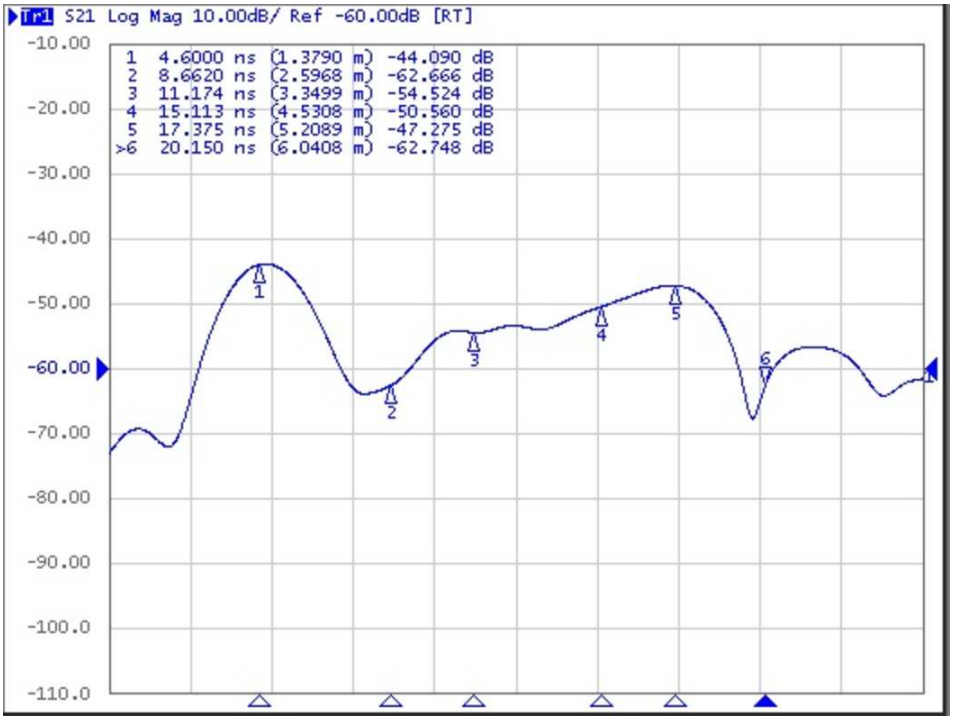


(b) Time domain response in the reverberation chamber with the diffusers.

Figure 4.6: Diagrams of the time domain response computed by the VNA.

# 5

# Results and Discussion

This chapter presents the experimental setups and procedures for the various experiments undertaken to reduce the unstirred energy. In order to test the conditions under which our diffusers work better (e.g. sequence, polarization, angles) the experiment took place initially in the anechoic chamber. There we were able to test the differences between the specular reflection and the scattered reflection having subtracted the direct path radiation. The benefit of the anechoic chamber is the minimization of the multi-path reflections from the walls due to the absorbers. The results of these experiments are presented in section 5.1.

Later, and based on the preliminary results of the anechoic chamber, the same experiments took place in the more complex environment of the reverberation chamber. These experiments allowed us to compare the unstirred and the stirred energy with or without the diffusers in the room.

## 5.1 Measurements in the Anechoic Chamber

The first stage of the experiments is based on the performance of the diffusers in the anechoic chamber. According to the simulations in MATLAB, it is expected that the scattering of the energy will be obvious when the antennas are at the same angles. Also the results will be more efficient around the critical frequency ($\sim$ 3GHz) based on which the diffusers were constructed. Two sets of measurements are performed using ridged horn antennas at different angles; one with the diffusers placed on the floor between the antennas and one with the plane reflector. For each set of measurements, the values of the channel transfer function are collected using the procedure described in chapter 4. The frequency range was set from 1.5GHz to 8.5GHz. Both the antennas and the absorbers of the chamber operate satisfactorily over this range.

The strongest of the radiations that reaches the receiver is the one that follows the direct path between the two antennas. However, this signal does not interact with the diffusers or the reflecting plane on the floor. For this reason we firstly took a measurement of the direct path component as described in section 4.2. The estimated radiation has been subtracted for all the following measurements and plots.

One of the points we want to investigate is how the polarization of the diffusers regarding the incident electric filed (Transverse Magnetic mode-TE) affects the measurements. For this reason, we took measurements for three different positions of diffusers a) the diffusers are placed perpendicularly to the incident electric field, b) the diffusers are placed parallel and c) the diffusers are set at 45 degrees. Keeping fixed the position of the diffusers, we move the antennas to different angles in order to investigate if there are preferable positions where the results are more efficient.

### 5.1.1 Diffusers placed perpendicularly

In this section we study the case where the diffusers are placed perpendicularly to the incident electric field. In Figure 5.1 the antennas are both placed in intermediate angles of $50^o$. Theoretically, we expect the specular reflection to be stronger when both antennas are at the same angle and, as a result, the reduction due to the diffusers to be higher. Generally, it is observed that the level of the power that is reflected from

the diffusers (red line) is lower than the one reflected from the plane reflector (blue line). The higher reduction is shown at $\sim$ 3GHz and at $\sim$ 6GHz while, in contrast, the smaller one is found at $\sim$ 4.5GHz and at $<$ 2GHz.

As expected, the first minimum is found at the critical frequency of $\sim$ 3GHz due to the $\lambda/4$ construction of the diffusers based on this frequency. The second minimum is at $\sim$ 6GHz. This is not unexpected as the second minimum corresponds to the half wavelength of the first one meaning that again our diffusers sequence should work efficiently adding the same phase to both wave bands. The only difference is that the smaller wavelength (higher frequency) will 'see' more diffusers on the plane - specifically, double number of diffusers. This fact is also presented in our results by the $\sim$ 15dB difference between the two minimum and their different widths. Going back to our MATLAB simulations, we can see the same results comparing the plots for same angles but different number of diffusers. Moving from 10 to 20 diffusers, the range of efficiency becomes more narrow while the reduction of the specular reflection increases. It seems that using more diffusers may increase the reduction of the specular energy but it will work for a more narrow frequency band.

In contrast to these frequencies, at the regions $<$ 2GHz and $\sim$ 4.5GHz both the specular reflected and the scattered radiation have the same power. This can also be explained easily by comparing the wavelength of these regions with the critical one. The $\sim$ 4.5GHz corresponds to $2\lambda_{cr}/3$ wavelength which means that is has a phase difference with the critical wavelength of $\pi/3$. The diffusers based on their $\lambda_{cr}/4$ contraction will induce a further phase of $\pi$ and so the total induced phase will be $4\pi/3$. This will maximize the reflection level power comparing to the previous frequencies. The same method should also work for the $<$ 2GHz region.

This could be a general estimation and explanation of the minimum and maximum differences that we expect to see at the different frequencies. But how could we have a more accurate prediction? Based on our analysis in section 3, it is easy to estimate the delay for a well to the next one if the transmitting and the receiving angles are known. In this case, when the delay induces a phase $\pi$ we expect to have a minimum, while when it induces a phase $2\pi$ we expect to have a maximum. As the width of the diffusers is fixed at $\lambda/4$ of the $\sim$ 3 GHz frequency, the specific contraction will induce

different phases to the rest of the frequencies we are using. Theoretically, we expect to find a minimum reduction for the frequencies with an odd multiple of the $\lambda_{cr}/2$ and a maximum for the ones with an even multiple. However, for the estimation of the specific frequencies we have to take into account the angle of reflection as well. In the case that both antennas are placed at the same angles, the above analysis could be summarized in the following equation:

$$f = 2 * (c/n * 0.025/\cos(\theta))/10^9 \tag{5.1}$$

where for $n = 1, 3, 5, ...$, $f$ are the frequencies in GHz with the maximum reduction of the specular reflection, while for $n = 2, 4, 6, ...$, $f$ are the frequencies with the minimum reduction. The rest of the parameters are: $\theta$ is the reflection angle (measured from the normal), 0.025m is the width of the diffusers we are using and $c = 3 \times 10^8$m/s the speed of light.

For the example of Figure 5.1 the above equation gives us $f = 2.0,\ 2.6,\ 3.6,\ 6.1$ GHz etc the frequencies where the radiation reaches the receiver in anti-phase due to the diffusers and we expect maximum reduction of the specular radiation. The same equation for $f = 1.8,\ 2.3,\ 3.1,\ 4.6$ GHz etc gives us the radiation that reaches the receiver in phase and we expect minimum reduction of the specular radiation. These results are in a perfect agreement with our experiment. The two strongest minima are found at 3.6GHz and 6.1GHz and there is a maxima at 4.6GHz as well. For frequencies $<$ 3GHz the step between maximum and minimum is too small and is difficult to see clear results. Taking also into account the errors that could arise from our experiments (e.g. estimation of the reflected angle using the wooden contraction, diffuser's placement at accurate distances) the results are more than encouraging.

The results, when both antennas are placed at the same intermediate angles, showed that the method works perfectly, reducing the specular radiation by $\sim$ 5dB or even $\sim$ 20dB at the critical wavelength and their multiples. The next step is to study the results of our method when the antennas are placed in different angles.

Since our model accurately predicts the results of our experiment, maybe there is no need to take more measurements when both of the antennas are placed at the same angles. However, there are still parameters that we have not been taken into account.

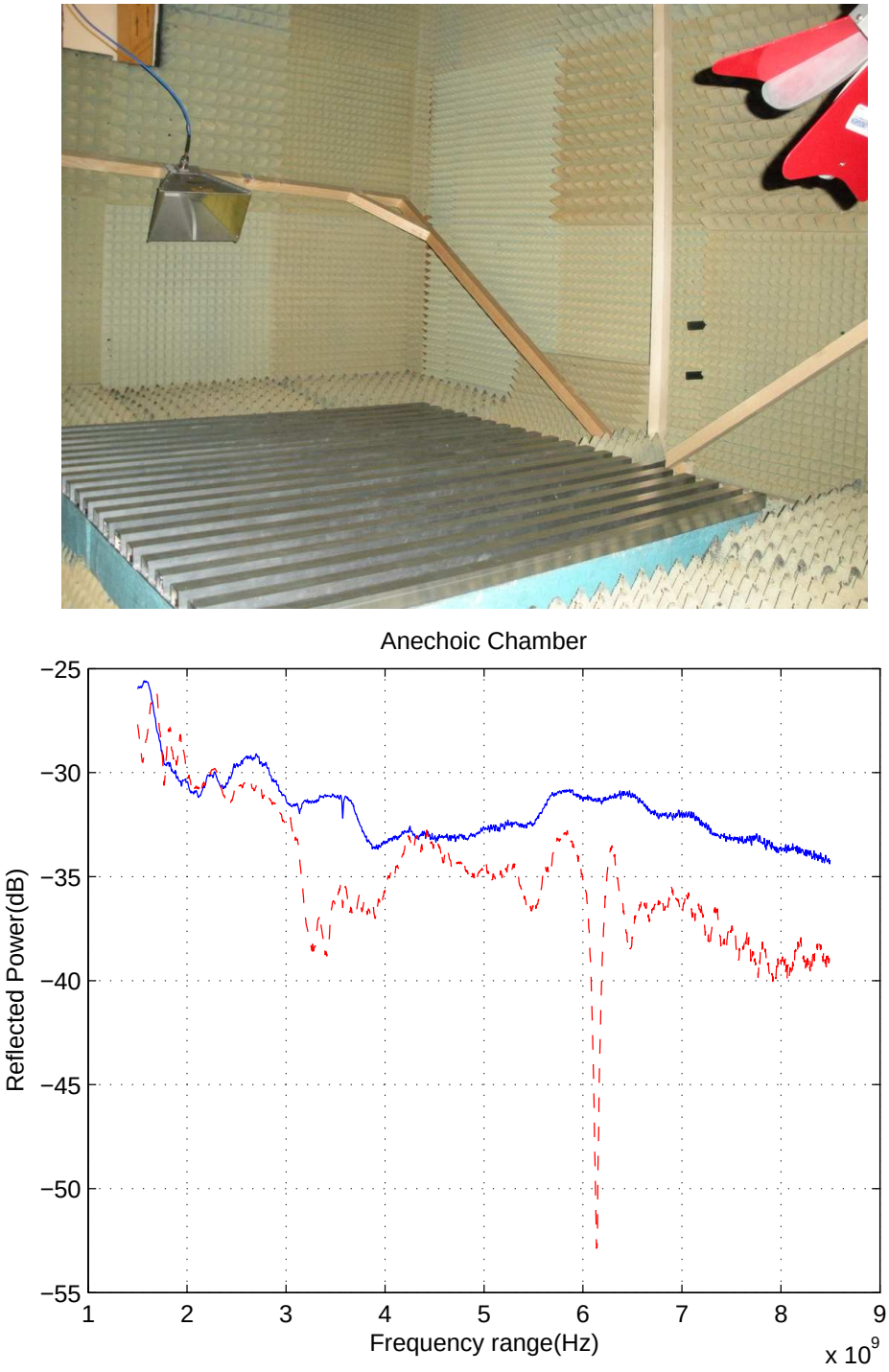


Figure 5.1: Top: Measurement setup where both antennas are placed at 50 degrees. The diffusers are also shown on the floor between the antennas and perpendicularly to them. Bottom: Reflecting power as a function of frequency. The red line represents the average reflected power from the diffusers and the blue one the average reflected power from the plane reflector.

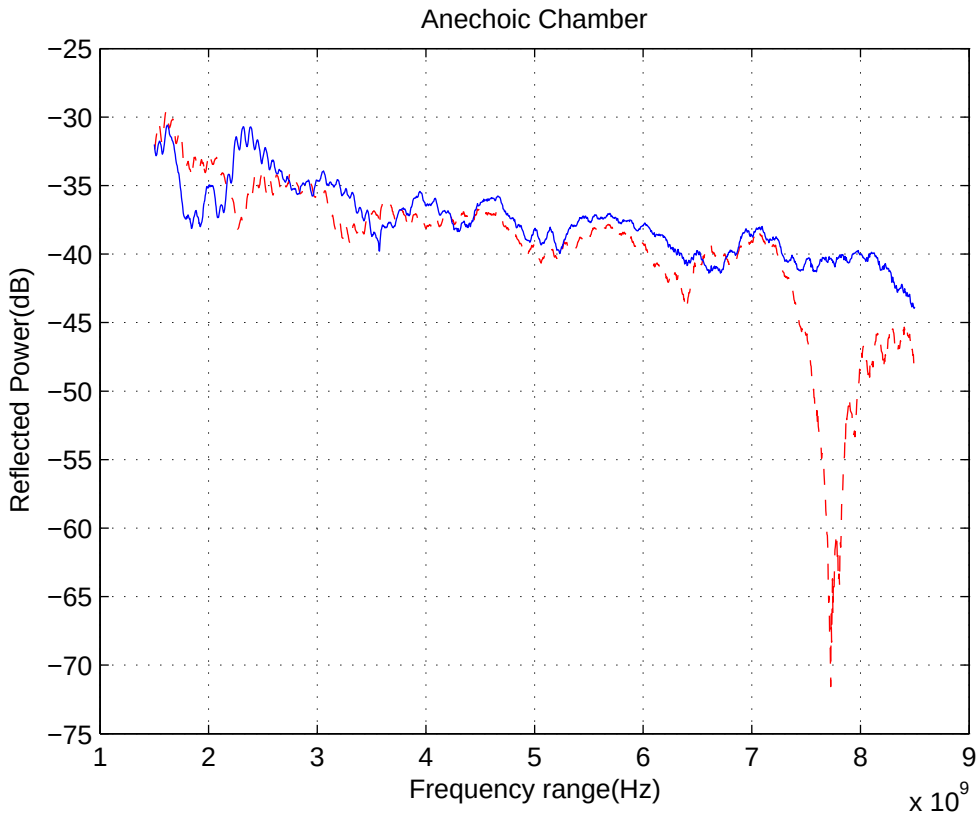


Figure 5.2: Reflecting power as a function of frequency for both antennas placed at 80 degrees. The red line represents the average reflected power from the diffusers and the blue one the average reflected power from the plane reflector.

One of them is the distance of the antennas from the center of the diffusers and the other one is their orientation. Figure 5.2 shows an example of both antennas placed at $80^o$. Moving the antennas from smaller to bigger angles(measuring the angles from the surface) the efficient part of the diffusers becomes smaller. Due to their directionality and the distance we use, the antennas at $80^o$ see less gratings than the $50^o$. As it has been explained, when the number of gratings is smaller lower reduction is expected around the critical frequency. The efficient frequencies for the case of $80^o$ are around 3.3, 4.7 and 7.8GHz. In Figure 5.2 we see a clear minimum at 7.8GHz and a smaller one at 3.3GHz. As the smaller wavelengths(higher frequencies) 'see' more gratings than the bigger ones our results could be probably explained from the above analysis.

If these two results are not strongly affected from errors or other parameters that we have not taken into account we could conclude to the followings:

- Our method for reducing the specular radiation works quite satisfactorily around

the critical frequency of 3GHz especially when moving the antennas to smaller angles.

- The diffusers work also efficiently for frequencies with even multiple wavelength of the $\lambda_{cr}/2$.

- Our results and the performance of the diffusers could be improved on 3 ways a) increasing the number of the diffusers (not possible in our case due to the limited space), b) increasing the distance of the antennas from the diffusers (again not possible for the same reason) and c) replacing the ridged horn antennas that are characterized by high directivity by omni-directional circular biconical antennas to detect as many reflections as possible when performing our method in the reverberation chamber.

### 5.1.2 Diffusers placed in parallel

The next step of our research was to study the diffusive properties when the diffusers are placed in parallel to the incident electric field. The measurement setup is shown in Figure 5.3. Theoretically, we expect to see no difference between the specular reflection and the diffused. In reality, when the diffusers are placed in parallel there is no diffusion because the only delay between two waves is the distance between them just like in the case of specular reflection. Our experiments agree with this prediction for all the possible combinations of angles for the transmitter and the receiver. Figure 5.4 shows as an example, the results of our measurements for the cases that both the antennas are placed at 40 and 80 degrees respectively. It is clear for both cases, despite some exceptions, that both lines have the same form. In the left plot at 40 degrees, there is a small difference around 3GHz but not in the case of 80 degrees. Also, at any other frequency there is no evidence for a clear reduction. Comparing all our results where the diffusers are placed in parallel, the idea of the reduction due the diffusion is not strongly supported apart from same isolated cases like the one at 40 degrees. However, even in this case the reduction is not significant.

At this point it is important to observe figures 5.2 and 5.4 right. In both of these figures the blue line represents the reflected power from the plane reflector while the

Figure 5.3: Measurement setup where both antennas are placed at 40 degrees.

antennas are at 80 degrees. It is obvious that these blue lines have some similarities but they are not identical. This is why from day to day the reference line was different because the experiment was highly sensitive to many parameters like the exact position of the antennas and the diffusers. However, the reliability of the method is not disputable because the current research focuses on the difference between the reflected power from the plane reflector and the diffusers. For every different case that was tested out (different angles, orientations of the diffusers e.t.c) the comparison of the received power with and without the diffusers was performed under the same exactly conditions.

### 5.1.3 Diffusers placed at 45 degrees

The logical next stage of the experiments was to place the sequence of the diffusers in a different orientation. For this step we chose an intermediate angle at 45 degrees. In order to explain the results it is important to understand which is the additional parameter which is induced to our experiment by the the orientation of the diffusers. Obviously, this case is more complex than the previous one and a simple prediction based on a 2-D model of radiation is not enough. In Figure 5.5 we are trying to show

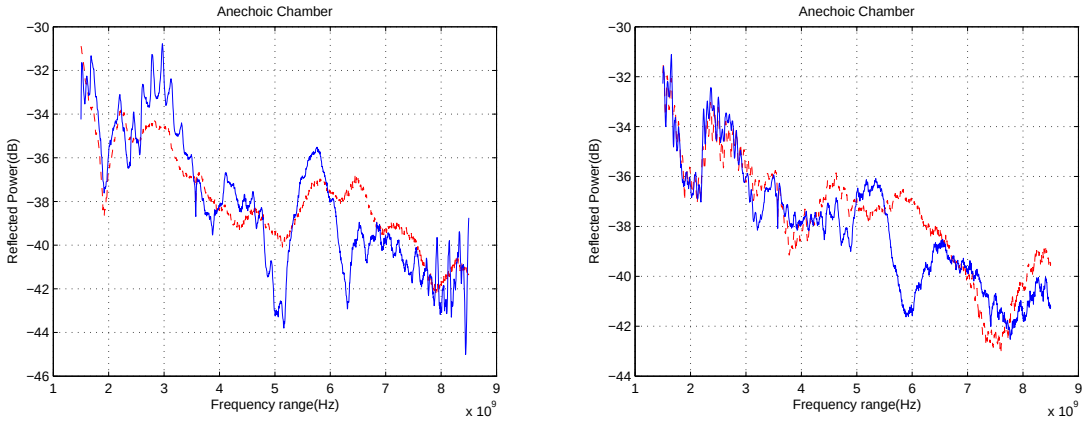


Figure 5.4: Reflecting power as a function of frequency. Left: Both antennas are placed at 40 degrees. Right: Both antennas are placed at 80 degrees. The red line represents the average reflected power from the diffusers and the blue one the average reflected power from the plane reflector.

a schematic representation of the wave diffusion when the orientation of the diffusers is 45 degrees and compare it with the case of perpendicularly orientation.

We assume two planes on the diffusers represented by a solid black line, call it 'A', and a dashed black line, call it 'B', whose distance is $n\lambda/4$ where $n = 1, 3, 5....$ If the diffusers where placed perpendicularly, these two levels would represent a grating and gap respectively. Now, lets assume two waves (red and green) that reach the two planes A and B at different positions again with distance $n\lambda/4$. In the case of perpendicular diffusers, all the waves that reach the same plane will be in phase and will reach the receiver the same time. In contrast, for the case of the 45 degrees orientation, the two waves (red and green solid lines) are in anti-phase with the red ones having a delay $\lambda/2$ due to the diffusers. As a result, the green waves will reach the receiver before the red ones despite both of them come from the same plane 'A'. Comparing this case to the one with the perpendicular diffusers, an additional delay due to the orientation is added apart from that due to the diffusers. Turning the diffusers at the 45 degrees, we increase the number of the waves in anti-phase and as a result we increase the scattering. In this case, we expect the result under the specific orientation to be more significant compared to the perpendicularly orientation.

Figure 5.6 shows our results in this condition with the antennas at 80 and 40 degrees. The remarkable result is that with this specific orientation of the diffusers we are able to achieve a total reduction of the specular reflection over almost all the

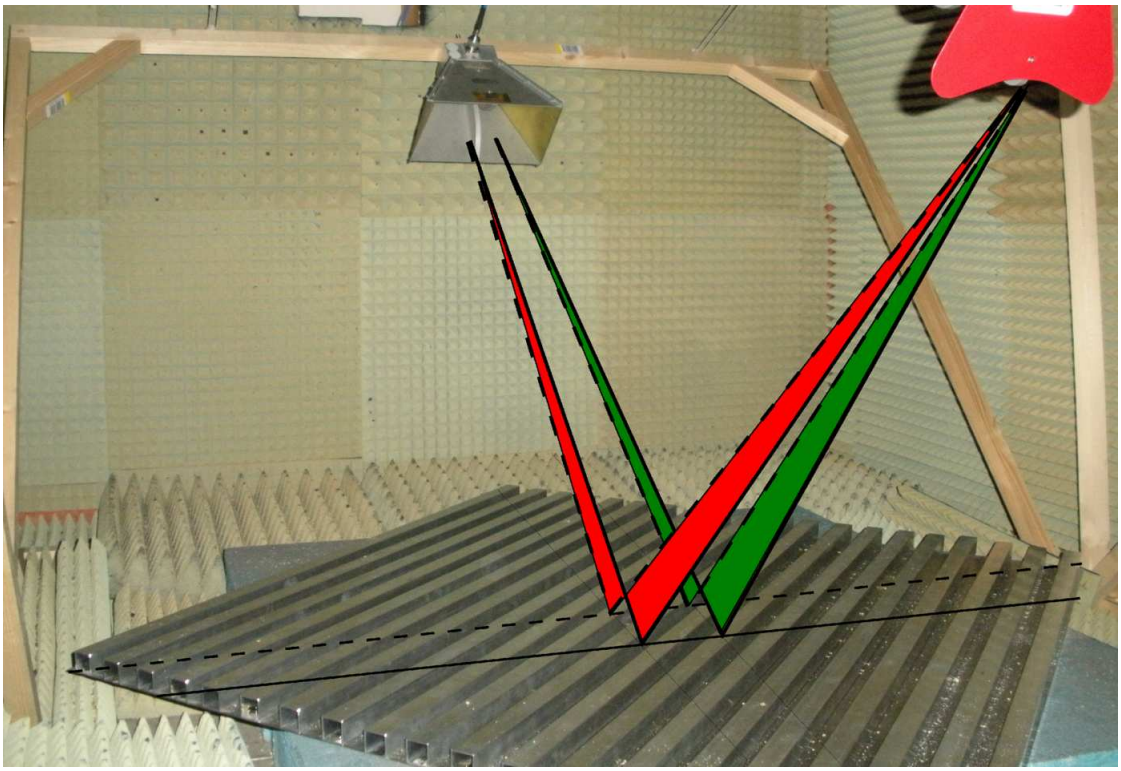

Figure 5.5: A schematic representation of wave diffusion when the orientation of the diffusers is 45 degrees.

frequency range. The reduction at $\sim$ 3GHz is significant for both cases in contrast with the perpendicularly diffusers where the results for larger angles were not so clear.

As our model seems to work better for 45 degree orientation of the sequence we investigated further this case taking measurements when placing the antennas at different angles. Figure 5.7 shows an example where the transmitter is stable at 60 degrees position and the receiver is moving from 30 to 90 degrees with a step of $10^o$. Due to the size of the chaber it was impossible to take measurements for angles lower than 30 degrees. It is obvious that the reduction of the specular reflection around the 3GHz increases with the receiver angle. Significant reduction is also observed around 7 and 8.5GHz. The specific frequency values slightly change depending on the receiver's position.

A possible explanation of our results could be given based on Lambert's cosine law (Lambert, 1760). Based on the so-called cosine emission law, the radiant intensity from an ideal diffusely reflecting surface is directly proportional to the cosine of the angle between the observer's line of sight and the surface normal. For our example, the surface normal is the same for all the cases and thus, the diffused reflection depends

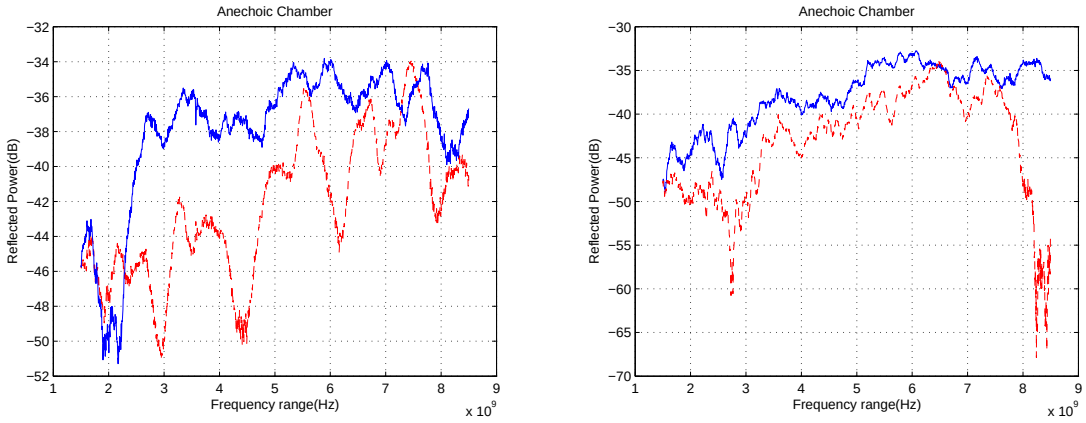


FIGURE 5.6: Reflecting power as a function of frequency. Diffusers are places at 45 degrees. Left: Both antennas are placed at 40 degrees. Right: Both antennas are placed at 80 degrees. The red line represents the average reflected power from the diffusers and the blue one the average reflected power from the plane reflector.

only on the receiver's angle. Despite our surface is not an ideal diffusely one, it seems that our results follow the Lambert's law and the diffusion is more efficient at higher angles (we estimate the angle from the ground and not from the surface normal).

## 5.2 Measurements in the Reverberation Chamber

At the last stage of our experiments, all the considerations done in the previous sections need to be validated by measurements in the reverberation chamber in order to test our method of reducing the unstirred energy. As the reverberation chamber creates a complex environment due to the multiple reflections, in order to determine the accuracy of our method, several measurements are needed. During our tests, the parameters which could affect our results (e.g. the heights of the antennas, their polarizations and the orientation of the diffusers) were changed in a number of possible combinations. Regarding the positions of the antennas, we have to mention that in the case of the reverberation chamber, we were unable to use the wooden frame from the anechoic chamber which allowed each antenna to be set independently at any angle from the normal. Nevertheless, in the RC we tested our method for different heights and polarizations of the antennas.

All the measurements were taken using the vector averaging of the chamber response over a complete stirrer rotation using 100 positions. In order to observe the

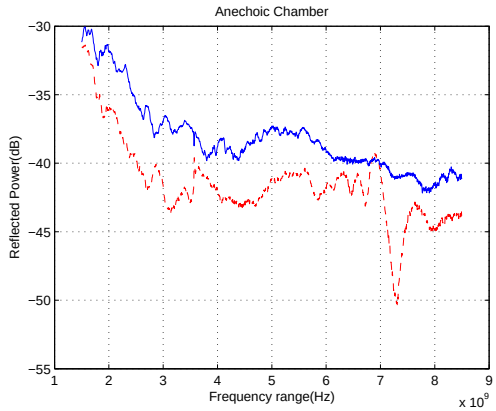


(a) Receiver at 30 degrees.

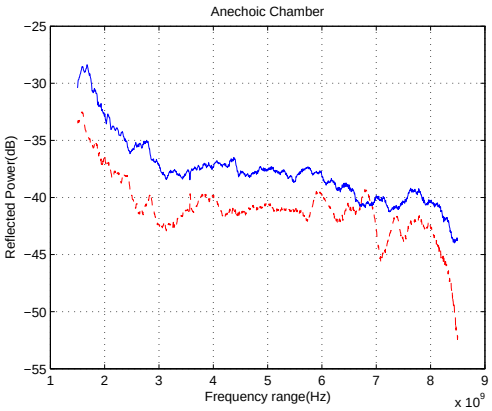


(b) Receiver at 40 degrees.

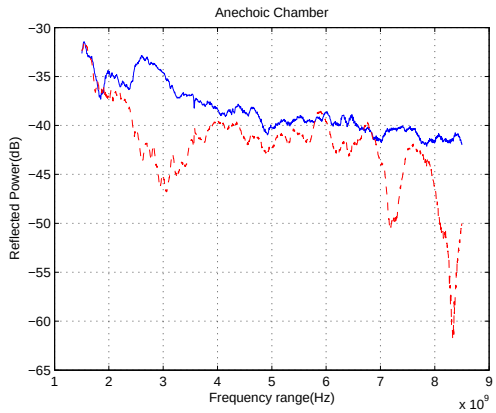


(c) Receiver at 60 degrees.

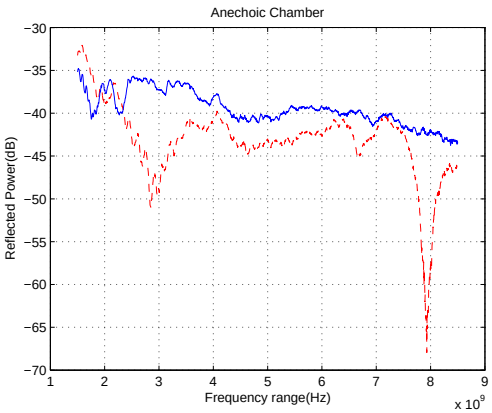


(d) Receiver at 70 degrees.

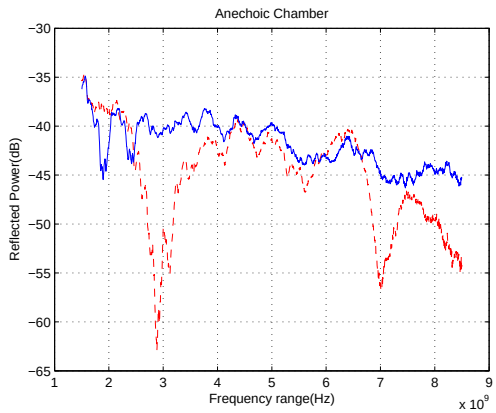


(e) Receiver at 80 degrees.

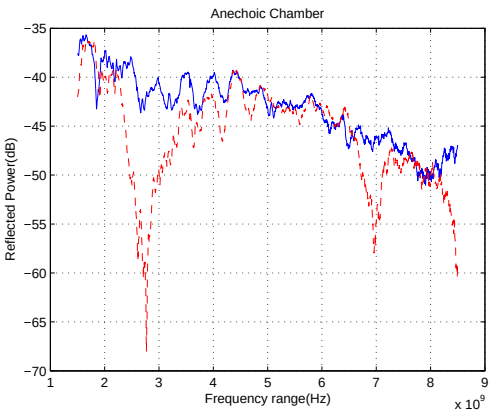


(f) Receiver at 90 degrees.

Figure 5.7: Reflecting power as a function of frequency. Diffusers are places at 45 degrees. Transmitting antenna is placed at 60 degrees while the receiver is moving from 30 to 90 degrees. The red line represents the average reflected power from the diffusers and the blue one the average reflected power from the plane reflector.

effect of the diffusers operating over a specific bandwidth the analyser frequency sweep was set to a frequency range of 2GHz to 4GHz with 1601 measurement points. This frequency range is a compromise between restricting the frequency range to that of the diffusers and having a sufficiently wide frequency range to give adequate time resolution, post transformation, that enables separation and thus identification of the individual specular reflection paths as mentioned in chapter 4. In order to improve further our results, we also took measurements for even narrower frequency ranges of 2.3-3.7GHz and 2.6-3.4GHz.

To optimize our results we used two methods. In the first one, we performed a smoothing of the results using the moving average method. The size of the sample that we used to in compute the average depends on the frequency range and has been selected in such a way to ensure that we do not lose any information of the total data. In the second method, we plot the standard deviation of our data within a frequency window. The goal of the performance of the present method is to optimise the uniformity of the field by eliminating the variations of the field from place to place. In other words, we expect that the standard deviation of the unstirred signal observed in the frequency domain should be reduced if the specular reflection contributions to the unstirred signal are reduced by the diffusers relative to the larger contribution from the direct path.

To begin with, Figure 5.8 (left) represents the experimental setup. In this case the heights of the antennas and the distance between them are 1m, so both of them had been placed at 60 degrees angle from the floor. Moreover, the frequency range was set to 2-4GHz and the diffusers have been placed perpendicularly to the incident electric field around the specular reflection areas, e.g. on the floor between the antennas, the walls and the floors behind them and on the ceiling. The plot on the right of the figure is a comparison of the received signal without (blue curve) and with the diffusers (red curve). It is observed that the energy reflected from the diffusers is lower around 3GHz. Narrowing the frequency band and approaching 3GHz, the results that came up are presented at the left and right plot of Figure 5.9 where the frequency range is 2.3-3.7GHz and 2.6-3.4GHz respectively. We see that the reduction around 3GHz reaches a maximum of -4dB. Comparing to respective results from the anechoic chamber and

studying the rest of the observed frequency range we see that this reduction is not significant.

Based on the results we received from the anechoic chamber, our method works better when the diffusers are placed at 45 degrees orientation. For this reason, we also took measurements for the same positions of the antennas (1m distance and 1m height) but with 45 degree orientation of the diffusers. Under these circumstances, we got the results shown in Figure 5.10 for the three different frequency bands respectively. In agreement with our results from the anechoic chamber, it is clear that the scattering of the unstirred energy is more significant in these cases not only around the frequency of 3GHz, but also around all the frequency range with some exceptions while the red line that represents the averaged received power from the diffusers is significantly lower than the blue one that represents the reflected averaged power from the plane reflector comparing with the case where the diffusers were placed at horizontal position.

At the next stage of our experiment, we kept the receiving antenna at 1m high and we placed the transmitting antenna at 0.5m. In this case the transmitting angle will be smaller ($45^o$ measured from the floor) compared to the receiving angle ($60^o$). We compare again the results from the same geometry when the diffusers are placed horizontally and when they are placed at 45 degrees. In Figure 5.11 we present the experimental setup when the diffusers are at 45 degrees. Their placement on the far wall and floor of the enclosure centered on the specular reflection points is visible in the image. The results of these two cases are shown in Figure 5.12. The frequency range of both cases is 2.6-3.4GHz.The diagrams confirm the success of our method to scatter the energy around the frequency of the diffusers.

Comparing these results with the previous case, where both antennas were placed at the same height, we see that we have achieved a further reduction of the unstirred energy about 7dB. Recalling the results of the anechoic chamber, we had concluded that the diffusion is more efficient when the receiver's angle from the normal is smaller than the transmitter's one. This is the case of the present comparison. Moving the transmitter to lower height we increase its angle from the normal and as a result we observe higher reduction of the energy. Comparing the plots in Figure 5.12 we could examine some conclusions for the effect of the diffuser's orientation in this case. The

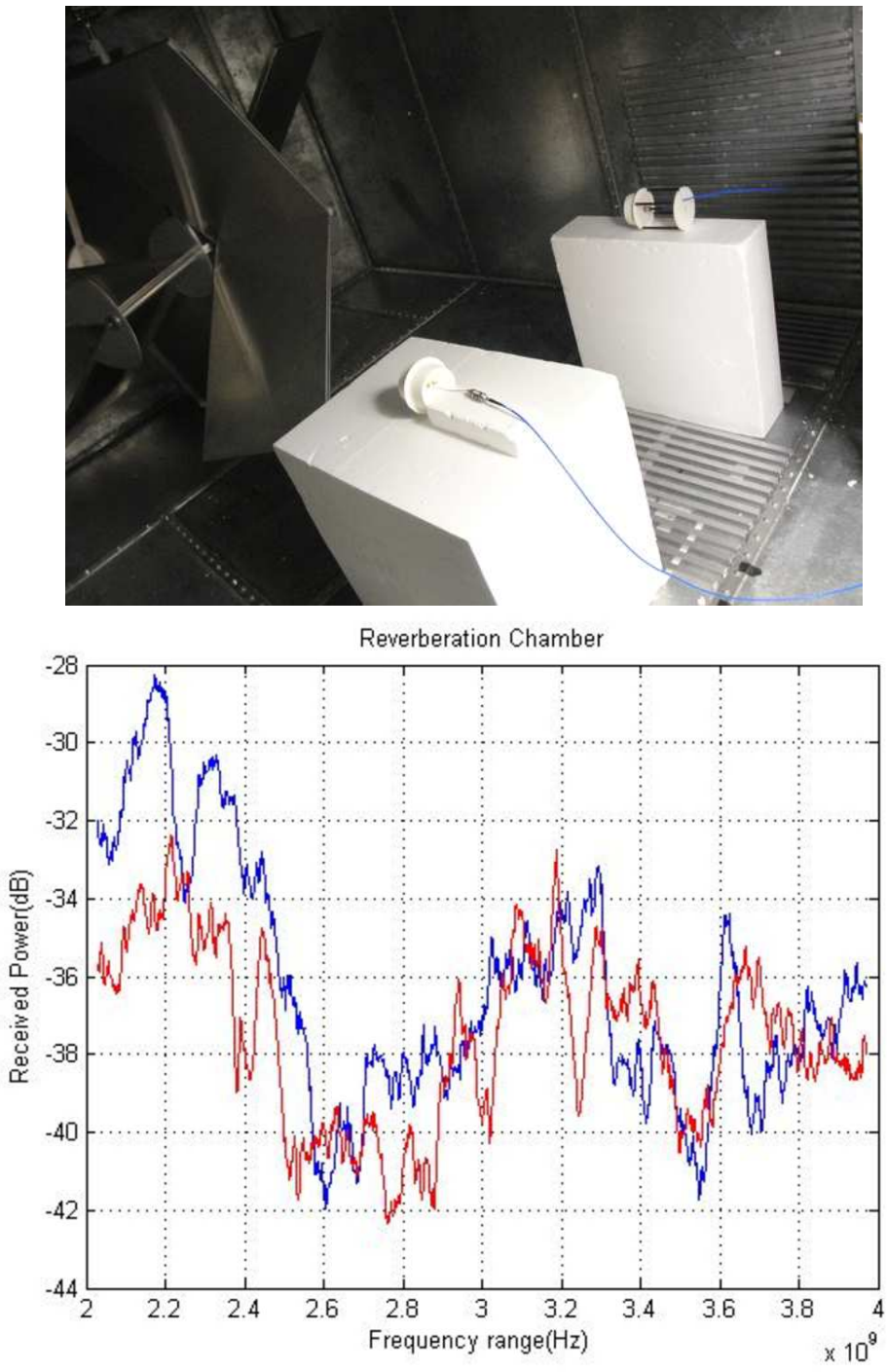


Figure 5.8: Top: Image of the Reverberation Chamber Interior showing antenna and diffusers placements. Antennas are placed at the same height (1m) and their distance is also 1m. Diffusers are placed at horizontal position. Bottom: Received power as a function of frequency for the showing placements. The frequency range is 2-4.7GHz. The red line represents the average reflected power from the diffusers and the blue one the average reflected power from the plane reflector.

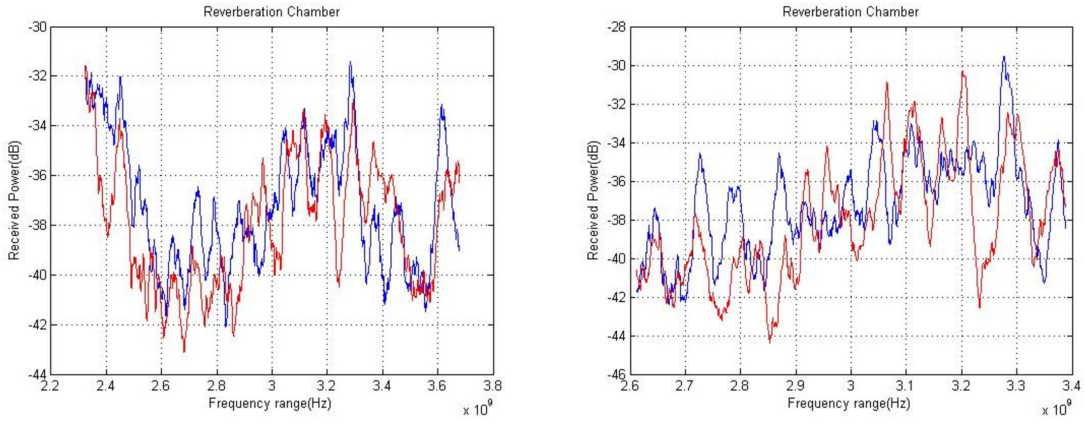


Figure 5.9: Received power as a function of frequency. Antennas are placed at the same height (1m) and their distance is also 1m. Diffusers are placed at horizontal position. The frequency range is 2.3-3.7GHz for the left plot and 2.6-3.4GHz for the right one.The red line represents the average reflected power from the diffusers and the blue one the average reflected power from the plane reflector.

blue curve represents the measurements in the chamber without diffusers. We could easily note that for both cases the blue curve is almost the same. Regarding the red line, apart from the fact that for both orientations the reduction of the unstirred energy around 3GHz is almost identical, in the case of 45 degrees orientation we see a further reduction also at higher frequencies. Based on these, we could assume that in this case, where the receiver is placed higher than the transmitter the orientation of the diffusers does not play a critical role for the reduction at the 3GHz. However, choosing the orientation of 45 degrees we may achieve a further reduction at the rest of the frequency range.

At the next step we placed the transmitting antenna at 1m height and the receiving antenna lower at 0.5m. In this case the transmitter's angle from the normal is smaller than the receiver's one. Again we keep the same geometry of the antennas changing the orientation of diffusers to 45 degrees. Our results are presented in Figure 5.13. For both cases we use a frequency range of 2.6-3.4GHz. In the left plots, where the diffusers are placed horizontally, it is obvious that there is no scattering of the unstirred energy, which is in agreement with the corresponding experiments in the anechoic chamber. In contrast, for the case of 45 degrees polarization, the reduction is obvious through the whole range of frequencies and particularly at 3GHz where is about -7dB like the previous case where the antennas were placed reversely. In agreement with our

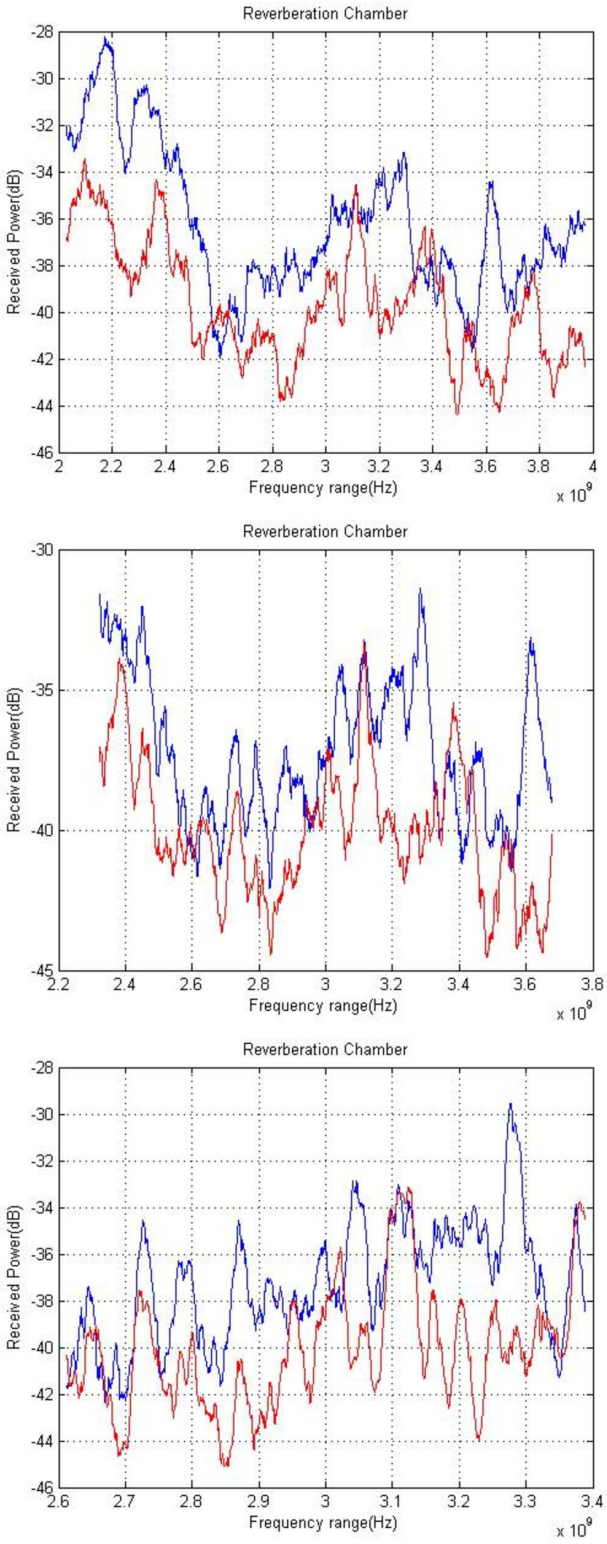


Figure 5.10: Received power as a function of frequency. Antennas are placed at the same heigh (1m) and their distance is also 1m. Diffusers are placed at 45 degrees orientation position. The frequency range is 2-4GHz, 2.3-3.7GHz and 2.6-3.4GHz from top to bottom. The red line represents the average reflected power from the diffusers and the blue one the average reflected power from the plane reflector.

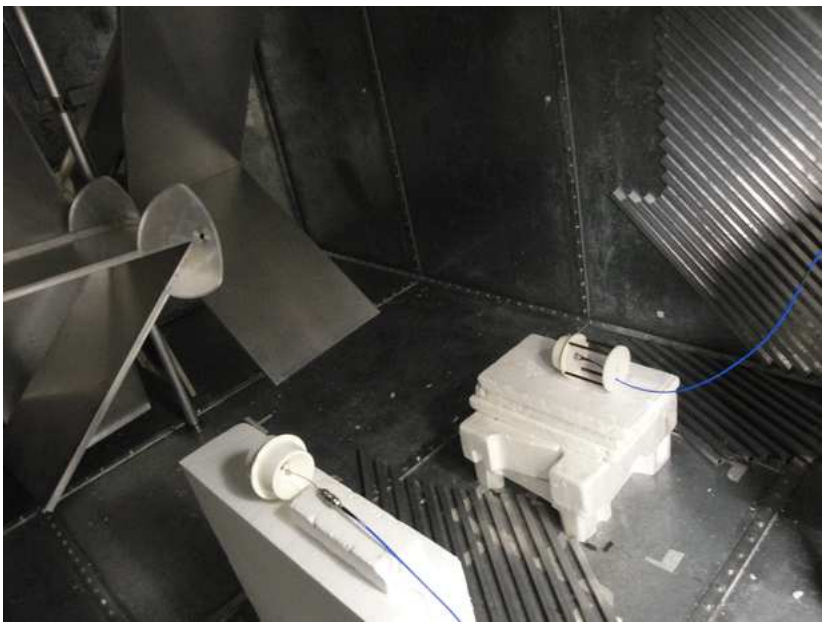

Figure 5.11: Image of the Reverberation Chamber Interior showing antenna and diffuser placement. The transmitter is placed at 0.5m and the receiver at 1.0m. The diffusers are placed at 45 degrees orientation. Their placement on the far wall and floor of the enclosure centered on the specular reflection points for the antenna is visible.

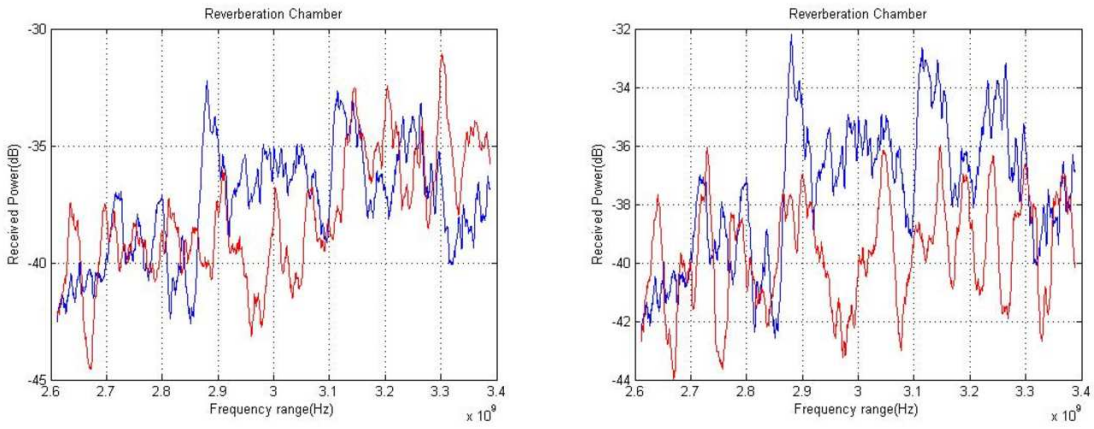


Figure 5.12: Received power as a function of frequency. The transmitter is placed at 0.5m and the receiver at 1.0m. Their distance is 1.0m. Diffusers are placed horizontally (left) and at 45 degrees (right) respectively. The frequency range is 2.6-3.4GHz. The red line represents the average reflected power from the diffusers and the blue one the average reflected power from the plane reflector.

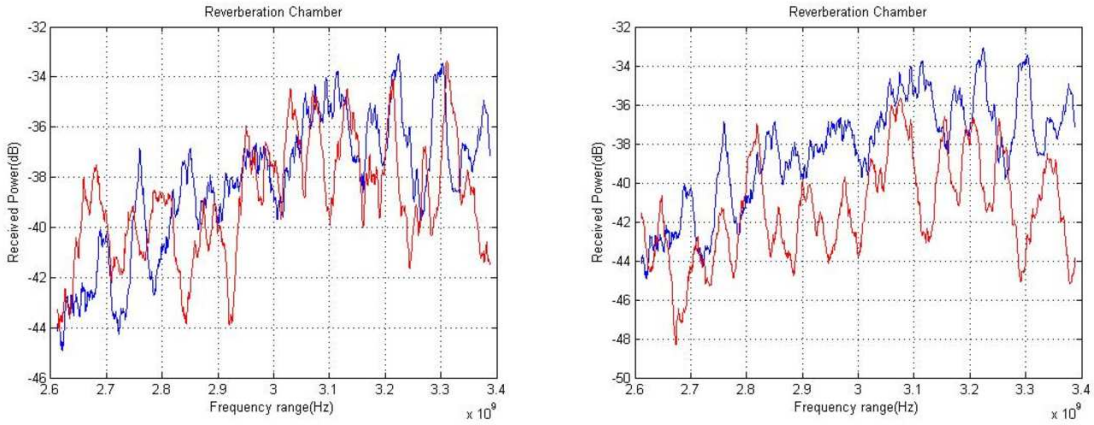


FIGURE 5.13: Received power as a function of frequency. The transmitter is placed at 1.0m and the receiver at 0.5m. Their distance is 1.0m. Diffusers are placed horizontally (left) and at 45 degrees (right) respectively. The frequency range is 2.6-3.4GHz. The red line represents the average reflected power from the diffusers and the blue one the average reflected power from the plane reflector.

previous conclusions, our method does not seem to work when the receiver's angle from the normal is higher than the transmitter's. The only way to improve the results in this case is to rotate our diffusers. In this case, our results seem to be independent of the antenna's position.

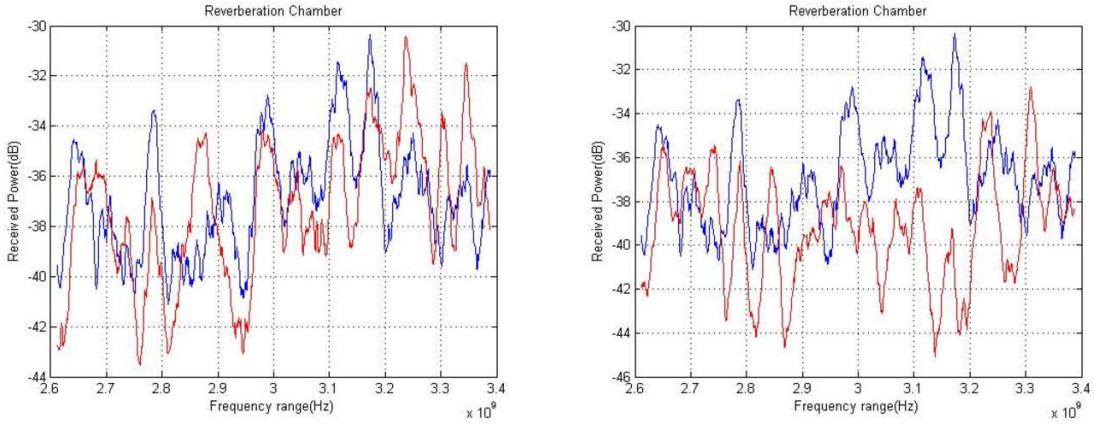


FIGURE 5.14: Received power as a function of frequency. Antennas are placed at the same height (0.5m) and their distance is 1m. Diffusers are placed horizontally (left) and at 45 degrees orientation position (right). The frequency range is 2.6-3.4GHz.The red line represents the average reflected power from the diffusers and the blue one the average reflected power from the plane reflector.

Finally, we placed both the antennas at the same 0.5m height. Figure 5.14 illustrates these results when diffusers are place perpendicular to the electric field and at 45 degrees orientation with the frequency range set at 2.6-3.4GHz. Comparing these two plots,

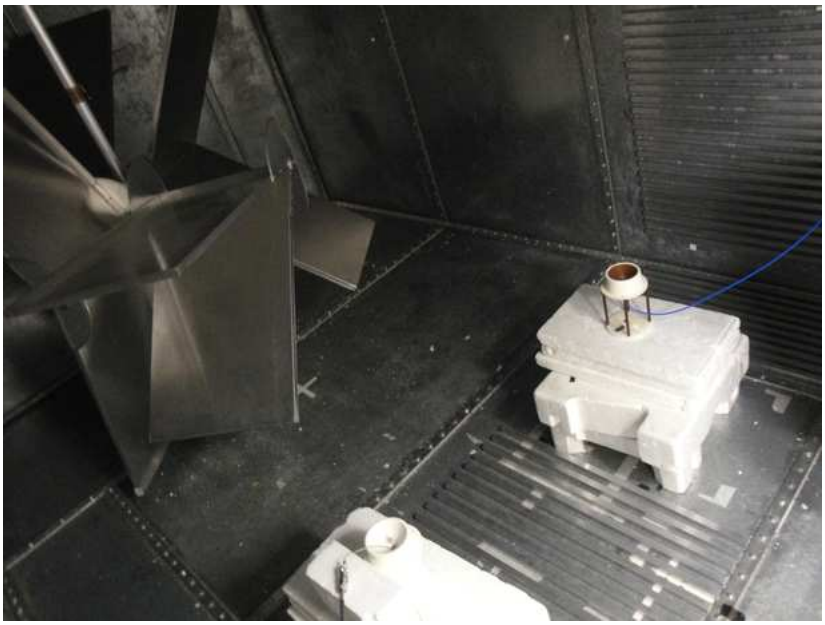

Figure 5.15: Image of the Reverberation Chamber Interior showing antenna and diffuser placement. The transmitter and the receiver are placed at 0.5m height while their orientation is parallel to the normal. The diffusers are placed horizontally.

we can see that with the sequence at 45 degrees there is scattering of the unstirred energy but not in the other case. We can also observe clear difference if we compare these results with the ones obtained when both antennas placed at 1.0m height.

At the next stage of our experiments we kept the heights of the antennas at 0.5m and we changed their polarization to vertical. The experimental setup when the diffusers are placed horizontally is shown in Figure 5.11. The results of this geometry and for frequency range 2.6-3.4GHz are presented in Figure 5.16. It is obvious that as in the case of the horizontal polarization, there is not scattering of the energy with the diffusers at this position. In contrast, for the case of 45 degrees orientation we see a significant reduction of the unstirred energy about to -14dB at the region of 3GHz.

In order to investigate further this case, we kept the antennas at the parallel to the normal position and the transmitter at 0.5m and we move the receiving antenna at 1.0m height. For the diffusers we use the classic two orientations. The results are shown in Figure 5.17. The frequency range is 2.6-3.4GHz. The results are expectable for the case of placing the diffusers perpendicularly based on the previous, no significant reduction is observed. However, the same results also came up for the 45 degrees orientation case, in contrast to the previous predictions where this orientation seemed to work better

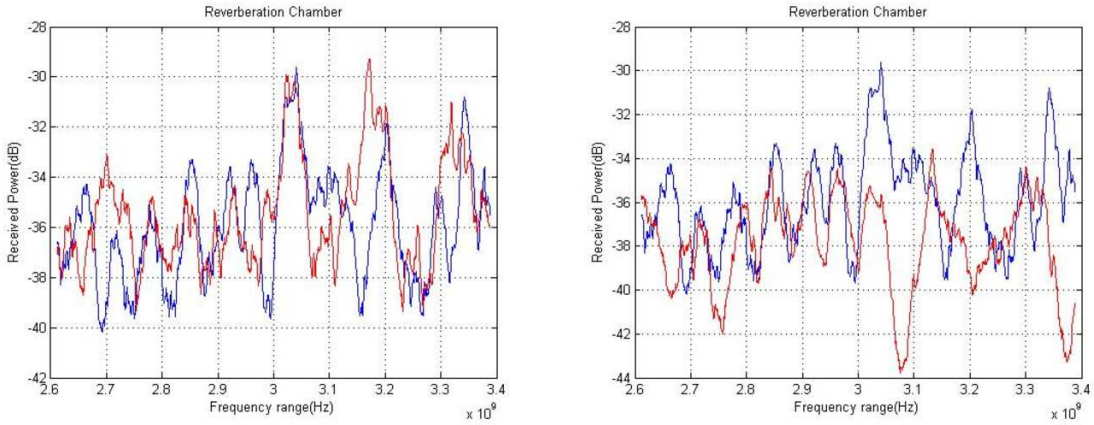


Figure 5.16: Received power as a function of frequency. Antennas are placed at the same height (0.5m) and their distance is 1m. Their orientation is parallel to the normal. Diffusers are placed horizontally (left) and at 45 degrees orientation position (right). The frequency range is 2.6-3.4GHz. The red line represents the average reflected power from the diffusers and the blue one the average reflected power from the plane reflector.

especially when the receiver was placed higher that the transmitter.

Placing the transmitter at 1m and the receiver at 0.5m with the diffusers at 45 degrees the results that came up are represented in Figure 5.18. In this case we can see that the energy is scattering around the critical frequency of 3GHz with a reduction of $\sim$ 4dB.

Finally, we placed both the antennas at 1m and the frequency range from 2-4GHz and 2.3-3.7GHz. The results for the diffusers perpendicular to the electric field are depicted in Figure 5.19 (left) and at 45 degrees (right). Comparing the plots, we note significant scattering of the unstirred energy over the whole frequency range at the 45 degrees in contrast to the other orientation.

### 5.2.1 Standard Deviation

In this section we present our results using the standard deviation of the data. This parameter is used to give a measure of the field uniformity in the reverberation chambers. In order to succeed the most possible accuracy of our results, we used shifted windows of 64 data. This gave us a total of 25 overlapping windows. Using the data of each one of the windows we estimated their standard deviation.

In Figures 5.20 - 5.22 we present a sample of three different experimental conditions where the standard deviation is plotted as a function of the observed frequency. Figure

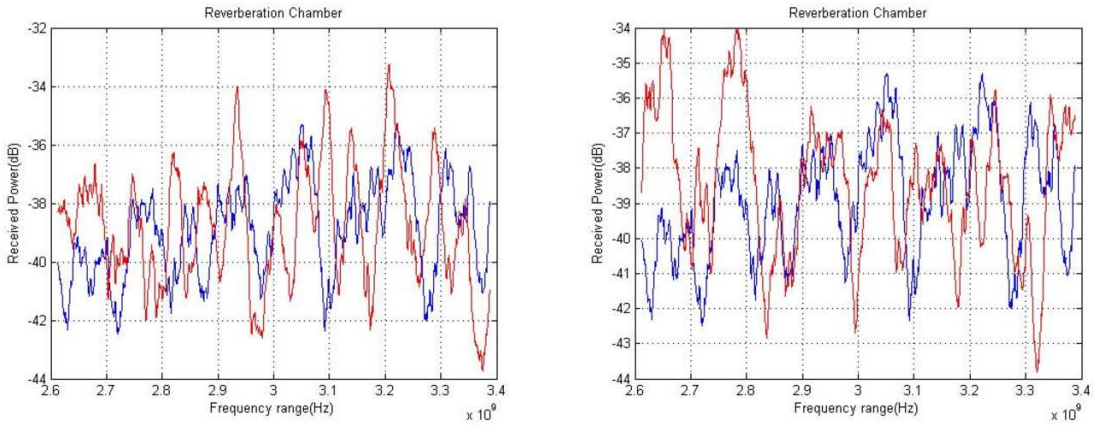


Figure 5.17: Received power as a function of frequency. The transmitter is placed at 0.5m height and the receiver at 1m. Their distance is 1m. The orientation of the antennas is parallel to the normal. Diffusers are placed horizontally(left) and at 45 degrees orientation position (right). The frequency range is 2.6-3.4GHz. The red line represents the average reflected power from the diffusers and the blue one the average reflected power from the plane reflector.

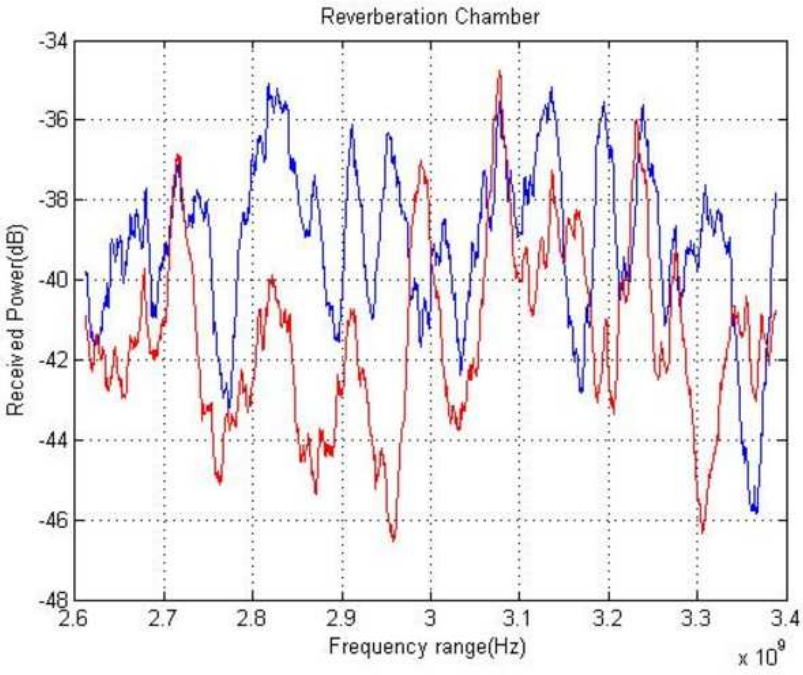


Figure 5.18: Received power as a function of frequency. The transmitter is placed at 1.0m height and the receiver at 0.5m. Their distance is 1m. The orientation of the antennas is parallel to the normal. Diffusers are placed at 45 degrees orientation position. The frequency range is 2.6-3.4GHz. The red line represents the average reflected power from the diffusers and the blue one the average reflected power from the plane reflector.

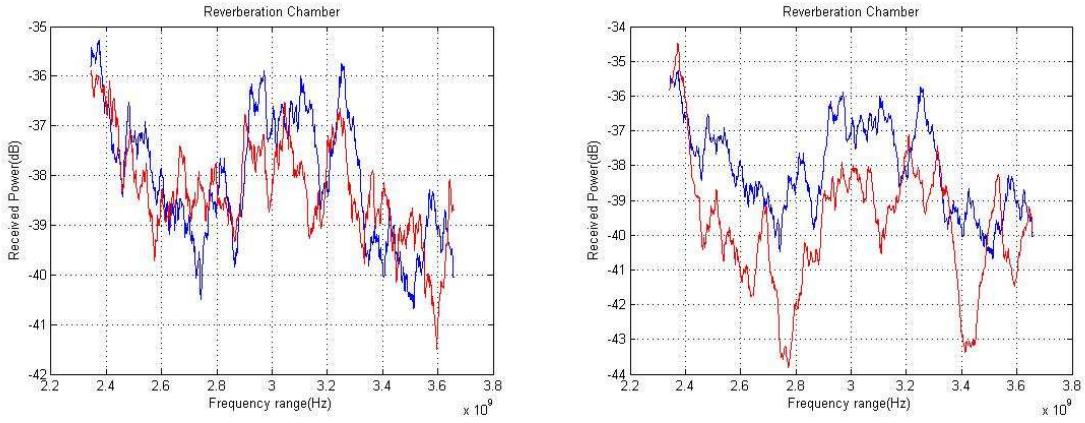


Figure 5.19: Received power as a function of frequency. Both antennas are placed at 1.0m height. Their distance is 1.0m. The orientation of the antennas is parallel to the normal. Diffusers are placed horizontally (left) and at 45 degrees orientation position (right). The frequency range is 2.3-3.7GHz.The red line represents the average reflected power from the diffusers and the blue one the average reflected power from the plane reflector.

5.20 shows the standard deviation of the received unstirred signal when both antennas are placed at 1.0m height, their orientation is vertical to the normal and the diffusers were placed at 45 degrees. It is clear that at the centre frequency of operation of the diffusers around 3GHz the standard deviation is significantly reduced whilst over the rest of the observed frequency range the two curves are comparable. The results that come up from these plots, are in agreement with the ones obtained from the same experiment setup 5.8

In Figure 5.21 we present the results of the same experimental setup but his time the transmitter has been placed at lower height than the receiver, at 0.5m. As expected from our previous results we note a significant reduction of the unstirred energy around 3GHz. In this case, the reduction seems to be even better than the previous one when the antennas were placed at the same height. This is an other confirmation that our method is more efficient when the transmitter is lower than the receiver.

Finally, Figure 5.22 depicts the standard deviation of the measurements taken when both the antennas were at 0.5m. However in this case the orientation of the antennas was in parallel to the normal. We observe a small reduction around 3GHz but this is significant. Generally as it has been noted from the plots of the data for the cases when the orientations of the antennas were in parallel to the normal, the reduction of the unstirred energy is not always significant.

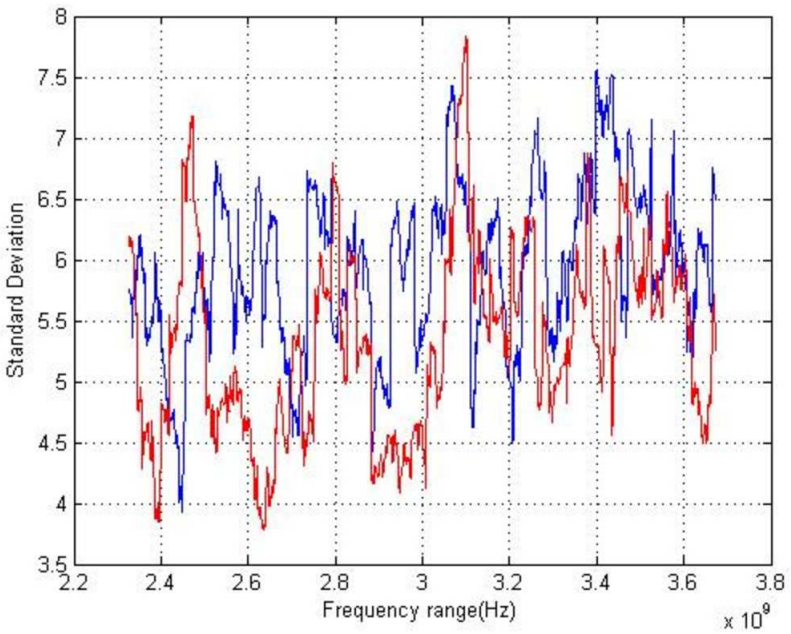


Figure 5.20: Standard deviation as a function of frequency. Both antennas are placed at 1.0m height. Their distance is 1m. The orientation of the antennas is vertical to the normal. Diffusers are placed at 45 degrees orientation position. The frequency range is 2.3-3.7GHz. The red line represents the average reflected power from the diffusers and the blue one the average reflected power from the plane reflector.

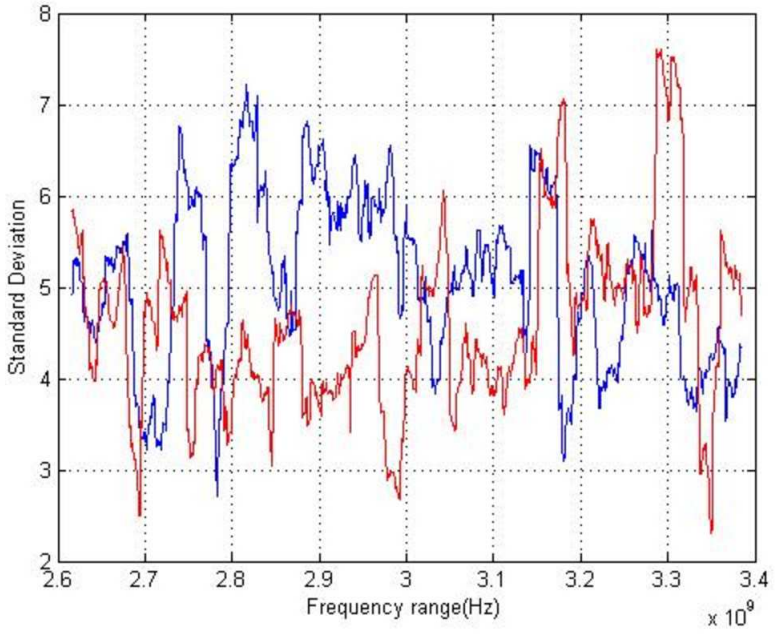


Figure 5.21: Standard deviation as a function of frequency. The transmitter is placed at 0.5m height and the receiver at 1.0m. Their distance is 1m. The orientation of the antennas is vertical to the normal. Diffusers are placed at 45 degrees orientation position. The frequency range is 2.6-3.4GHz. The red line represents the average reflected power from the diffusers and the blue one the average reflected power from the plane reflector.

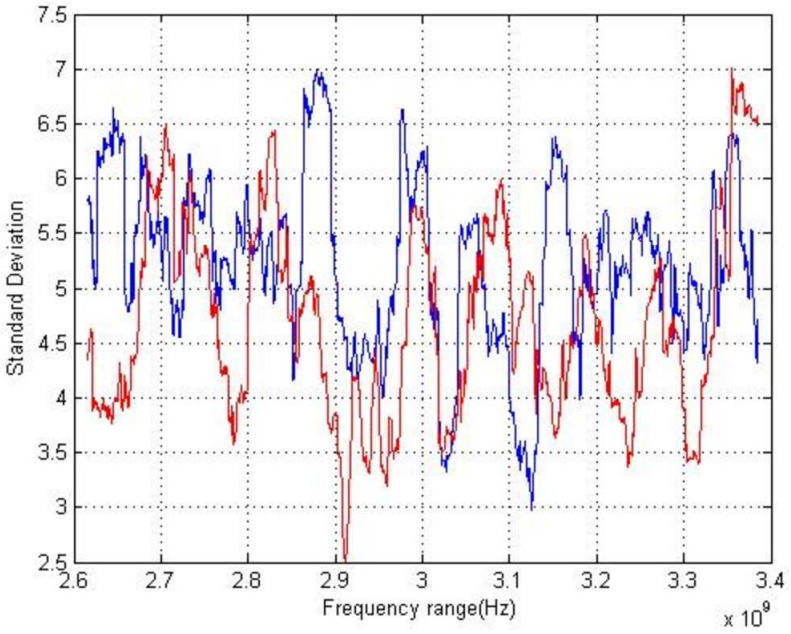


Figure 5.22: Standard deviation as a function of frequency. Both antennas are placed at 0.5m height. Their distance is 1m. The orientation of the antennas is parallel to the normal. Diffusers are placed at 45 degrees orientation position. The frequency range is 2.6-3.4GHz. The red line represents the average reflected power from the diffusers and the blue one the average reflected power from the plane reflector.

To summarize our results, it seems that placing the diffusers in the reverberation chamber causes scattering of the unstirred energy. Comparing the results to the ones of the anechoic chamber we could conclude that generally there is a good agreement. However, the measurements in the reverberation chamber tend to be more unpredictable. Therefore, we are not able to make a general assumption of how the the results depend on the different parameters we tested (e.g. position of antennas, polarization, orientation of the diffusers). However, there are some possible trends. Specifically, our model seems to work more efficiently when the diffusers placed at 45 degrees. Also the height of the antennas maybe plays a critical role, as in most cases we obtained better results when the receiver were higher or at least at the same hight with the transmitter. Based on our results, the preferred orientation of the antennas is the vertical to the normal. However, the most significant scattering of the unstirred energy was observed for a case where the antennas were placed parallel to the normal (see Figure 5.16). Despite that fact, the specific orientation does not show a uniform reduction for all the cases.

# 6

# Conclusions

This thesis work is based on the study of the use of wave diffusers in a reverberation chamber in order to reduce the unstirred energy. The unstirred energy, which is mainly contributed by specular reflections, arrives at the receiver without intersecting the stirrer. The role of the stirrer is to randomize the field, simulating a real environment, and to eliminate any deterministic component. When the unstirred energy is significant the randomized field is destroyed and that is way alternative methods are investigated in order to improve the stirred to unstirred ratio.

This thesis proposed the use of a well known method from the optics and acoustics, the use of wave diffusers. The proposal is that if the unstirred energy is scattered around in different directions then, the probability to interact with the stirrer in the chamber and become transferred to the stirred energy increases. If diffusers are placed at all specular reflection points then only the direct path between the antennas in the operating region of the chamber will remain for the unstirred energy. In practice

the total transfer of specular reflected energy from the unstirred energy to the stirred energy will not be possible and only a reduction in the specular reflected components of the unstirred energy will result.

Experimental validation was provided using both an anechoic and a reverberation chamber. The experiments made use of a simple two level periodic wave diffuser with a limited frequency bandwidth around the design frequency of 3GHz. The results from the anechoic chamber showed that our method works satisfactorily, reducing the specular reflation especially when the diffusers placed at $45^o$ to the transverse electric mode. Based on these results we tested our method also in the reverberation chamber where experiments showed a average extent of unstirred radiation reduction of $\sim$ 10dB. Depending on the conditions of the experiments, the results had demonstrated modest or more efficient success. Generally, the most significant results were found when the diffusers were placed at 45 degrees orientation and when the receiver's angle from the normal were smaller than the transmitter's one.

To conclude, the results from the present method can contribute to the development of techniques for mitigating the reverberation chambers unstirred field components. However, for even better performance of the chamber future research could focus on the use of different diffusers patterns. For instance, the use of 2D diffuser panels could provide more significant results. Finally further research in different sequences of diffusers that would affect different frequency ranges could provide more information on the scattering of the electromagnetic waves in the chamber.

# A

# Appendix

## A.1 Scattering simulation

```
%=============================================
% DiffuserSimulation.m
% Initialize modifiable parameters
clear
format compact
N=10; % Number of wells within the diffuser (prime> 2).
P=1; % Number of periods.
w=0.024; % Well depth (m) (e.g. λ/4).
f=3125*1000000; % Frequency (Hz).
c=3*(10^8); % Speed of light (m/s).
theta=0:0.01:pi/2; % Observetion angle.
```

```
phi=-60; % Source angle (degrees).
Hn=0;

%=============================================
% Flat plane scattering
for n=1:N*P
    Rn=1; % Reflection coefficient for plane surface.
    Hn=Hn+Rn*exp(-i*2*pi*f*n*w*sin(theta)/c)*exp(-i*2*pi*f*n*w*sin(phi*pi/180)/c);
end

%Hn=max(0,20*log10(abs(Hn)));
%polar(theta,Hn,'r') % Polar plot, obsercation angle vs. Amplitute
Hn1=abs(Hn);
plot(theta*180/pi,Hn1/max(Hn1),'b') % normalized Hn.
hold on

Hn=0;

%=============================================
%Diffusers scattering

for n=1:N*P
    if mod(n,2) == 0 sn=1;
    else sn=2; end
    dn=w*sn; % Well depth number n (m).
    if (dn>0) Rn=-(1+i*cot(2*pi*f*dn/c))/(1-i*cot(2*pi*f*dn/c));
    else isp('Well length of zero'), Rn=1; end
    Hn=Hn+Rn*exp(-i*2*pi*f*n*w*sin(theta)/c)*exp(-i*2*pi*f*n*w*sin(phi*pi/180)/c);
end
%Hn=max(0,20*log10(abs(Hn)));
%polar(theta,Hn,'r') % Polar plot, obsercation angle vs. Amplitute
```

```
Hn=abs(Hn);
plot(theta*180/pi,Hn/max(Hn1),'r') % normalized Hn.

title('Diffuser design', ['N=' num2str(N) ', w=' num2str(w) ', f=' num2str(f) 'Hz,
Source angle=' num2str(phi) 'deg' ])
ylabel('Normalized scattering factor')
xlabel('Observation angle (deg)')

legend( 'No diffusers','[+1 -1 +1 -1] sequence');
print -deps -color figure1.ps
```

# References


Arnaut, L. (2001). Operation of electromagnetic reverberation chambers with wave diffractors at relatively low frequencies. *Electromagnetic Compatibility, IEEE Transactions on*, 43(4):637 –653.

Arnaut, L. (2002). Compound exponential distributions for undermoded reverberation chambers. *Electromagnetic Compatibility, IEEE Transactions on*, 44(3):442 – 457.

Balanis, C. (1982). *Antenna theory: analysis and design*. Harper & Row series in electrical engineering. Wiley.

Cartet, R. G. (1990). *Electromagnetic waves*. Chapman and Hall,, London.

Choi, J.-H., Park, S.-O., Yang, T.-S., and Byun, J.-H. (2010). Generation of rayleigh/rician fading channels with variable rms delay by changing boundary conditions of the reverberation chamber. *Antennas and Wireless Propagation Letters, IEEE*, 9:510 –513.

Clegg, J., Marvin, A., Angus, J., and Dawson, J. (1996). Method for increasing the mode density in a reverberant screened room. *Science, Measurement and Technology, IEE Proceedings* -, 143(4):216 –220.

Corona, P., Ferrara, G., and Migliaccio, M. (1996). Reverberating chambers as sources of stochastic electromagnetic fields. *Electromagnetic Compatibility, IEEE Transactions on*, 38(3):348 –356.

Corona, P., Ferrara, G., and Migliaccio, M. (2000). Reverberating chamber electromagnetic field in presence of an unstirred component. *Electromagnetic Compatibility, IEEE Transactions on*, 42(2):111 –115.

Cox, T. and D'Antonio, P. (2009). *Acoustic Absorbers and Diffusers: Theory, Design and Application*. Taylor & Francis.

Crawford, M. L., Koepke, G. H., and States., U. (1986). *Design, evaluation, and use of a reverberation chamber for performing electromagnetic susceptibility/vulnerability measurements [microform] / M.L. Crawford, G.H. Koepke*. U.S. Dept. of Commerce, National Bureau of Standards ; For sale by the Supt. of Docs., U.S. G.P.O., Gaithersburg, MD : Washington, DC :.

D'Antonio, P. and Konnert, J. (1984). The reflection phase grating diffuser: Design theory and application. *Audio Engineering Society*.

Dawson, J. F., Hatfield, M. O., Arnaut, L., and Eulig, N. (2003). Reverberation (mode-stirred) chambers for electromagnetic compatibility. *EMC & Compliance Journal*.

Fielitz, H., Remley, K., Holloway, C., Zhang, Q., Wu, Q., and Matolak, D. (2010). Reverberation-chamber test environment for outdoor urban wireless propagation studies. *Antennas and Wireless Propagation Letters, IEEE*, 9:52 –56.

Giger, A. (1991). *Low-Angle Microwave Propagation: Physics and Modeling*. Artech House Telecommunications Library. Artech House.

Hammond, C. (2001). *The Basics of Crystallography and Diffraction*. IUCr texts on crystallography. Oxford University Press.

Hansen, T. B. (2012). Correlation and capacity calculations with reference antennas in an isotropic environment. *International Journal of Antennas and Propagation*.

Harima, K. (2005). Determination of emi antenna factor using reverberation chamber. In *Electromagnetic Compatibility, 2005. EMC 2005. 2005 International Symposium on*, volume 1, pages 93 –96.

Harrington, R. F. (1961). Time Harmonic Electromagnetic Fields.

Herring, J. L., Naylor, P., and Christopoulos, C. (1991). Transmission-line modelling in electromagnetic compatibility studies. *International Journal of Numerical Modelling-electronic Networks Devices and Fields*, 4:143–152.

Hill, D. (1994). Electronic mode stirring for reverberation chambers. *Electromagnetic Compatibility, IEEE Transactions on*, 36(4):294 –299.

Hill, D., Ma, M., Ondrejka, A., Riddle, B., Crawford, M., and Johnk, R. (1994). Aperture excitation of electrically large, lossy cavities. *Electromagnetic Compatibility, IEEE Transactions on*, 36(3):169 –178.

Hoijer, M., Andersson, A.-M., Lunden, O., and Backstrom, M. (2000). Numerical simulations as a tool for optimizing the geometrical design of reverberation chambers. In *Electromagnetic Compatibility, 2000. IEEE International Symposium on*, volume 1, pages 1 –6 vol.1.

Holloway, C., Hill, D., Ladbury, J., Wilson, P., Koepke, G., and Coder, J. (2006). On the use of reverberation chambers to simulate a rician radio environment for the testing of wireless devices. *Antennas and Propagation, IEEE Transactions on*, 54(11):3167 –3177.

IEC61000-4-21 (2003). Electromagnetic compatibility (emc) part 4-21:testing and measurement techniques reverberation chamber test methods. Technical report, International standard.

Jayaweera, S. and Poor, H. (2005). On the capacity of multiple-antenna systems in rician fading. *Wireless Communications, IEEE Transactions on*, 4(3):1102 – 1111.

Kouveliotis, N., Trakadas, P., and Capsalis, C. (2003). Theoretical investigation of the field conditions in a vibrating reverberation chamber with an unstirred component. *Electromagnetic Compatibility, IEEE Transactions on*, 45(1):77 – 81.

Lambert, J. (1760). *Photometria sive de mensura et gradibus luminis colorum et umbrae*. Vidvae Eberhardi Klett.

Leferink, F., Boudenot, J.-C., and van Etten, W. (2000). Experimental results obtained in the vibrating intrinsic reverberation chamber. In *Electromagnetic Compatibility, 2000. IEEE International Symposium on*, volume 2, pages 639 –644 vol.2.

Loughry, T. A. (1991). Frequency stirring: An alternate approach to mechanical mode-stirring for the conduct of electromagnetic susceptibility testing. Technical report.

Lunden, O. and Backstrom, M. (2007). How to avoid unstirred high frequency components in mode stirred reverberation chambers. In *Electromagnetic Compatibility, 2007. EMC 2007. IEEE International Symposium on*, pages 1 –4.

Mendes, H. A. (1968). A new approach to electromagnetic field- strength measurements in shielded enclosures. *Wescon*.

Peng, H., Guangjiong, S., Zhiming, S., Wei, L., Ningfeng, Z., and Xiang, Z. (2011). Influence of antenna configuration on the performance of the reverberation chamber. In *Cross Strait Quad-Regional Radio Science and Wireless Technology Conference (CSQRWC), 2011*, volume 1, pages 314 –317.

Petirsch, M. and Schwab, A. (1997). Optimizing shielded rooms utilizing acoustic analogies. In *Electromagnetic Compatibility, 1997. IEEE 1997 International Symposium on*, pages 154 –158.

Petirsch, W. and Schwab, A. (1999). Investigation of the field uniformity of a mode-stirred chamber using diffusers based on acoustic theory. *Electromagnetic Compatibility, IEEE Transactions on*, 41(4):446 –451.

Petirsh, M. and Schwab, A. (1998). Improving a mode-stirred chamber utilizing acoustic diffusers. In *Electromagnetic Compatibility, 1998. 1998 IEEE International Symposium on*, volume 1, pages 39 –43 vol.1.

Pirkl, R., Ladbury, J., and Remley, K. (2011). The reverberation chamber's unstirred field: A validation of the image theory interpretation. In *Electromagnetic Compatibility (EMC), 2011 IEEE International Symposium on*, pages 670 –675.

Price, R. H., Davis, H. T., and Wenaas, E. P. (1993). Determination of the statistical distribution of electromagnetic-field amplitudes in complex cavities. *Phys. Rev. E*, 48:4716–4729.

Primiani, V., Moglie, F., and Paolella, V. (2009). Numerical and experimental investigation of unstirred frequencies in reverberation chambers. In *Electromagnetic Compatibility, 2009. EMC 2009. IEEE International Symposium on*, pages 177 –181.

Primiani, V. M. and Moglie, F. (2010). Numerical simulation of los and nlos conditions for an antenna inside a reverberation chamber. *Journal of Electromagnetic Waves and Applications*, 24(17-18):2319–2331.

Rosengren, K. and Kildal, P.-S. (2001). Study of distributions of modes and plane waves in reverberation chambers for the characterization of antennas in a multipath environment. *Microwave and Optical Technology Letters*, 30(6):386–391.

Rosengren, K., Kildal, P.-S., Carlsson, C., and Carlsson, J. (2001). Characterization of antennas for mobile and wireless terminals by using reverberation chambers: improved accuracy by platform stirring. In *Antennas and Propagation Society International Symposium, 2001. IEEE*, volume 3, pages 350 –353 vol.3.

Schroeder, M. (1975). Diffuse sound reflection by maximum - length sequences. *Acoustical Society of America Journal*, 57:149–150.

Schroeder, M. (1985). *Number Theory in Science and Communication*. Springer-Verlag, Berlin, second edition.

Serra, R. (2009). *Introduction of Randomness in Deterministic, Physically-Consistent Descriptions of Reverberation Chambers and Experimental Verification*. PhD thesis, Politecnico di Torino, Turin, Italy.

Shuang-gang, L., Zhi-jie, W., and Jia-dong, X. (2009). Source stirring reverberation chamber design and experimental investigation. In *Microwave Conference, 2009. APMC 2009. Asia Pacific*, pages 1254 –1257.

Spiegelaar, H. and Vanderheyden, E. (1995). The mode stirred chamber-a cost effective emc testing alternative. In *Electromagnetic Compatibility, 1995. Symposium Record., 1995 IEEE International Symposium on*, pages 368 –373.

Stuber, G. L. (1996). *Principles of Mobile Communication*. Kluwer Academic Publishers, Norwell, MA, USA, 1st edition.

Wu, D. and Chang, D. (1989). The effect of an electrically large stirrer in a mode-stirred chamber. *Electromagnetic Compatibility, IEEE Transactions on*, 31(2):164 –169.